DESIGN AND HARDWARE IMPLEMENTATION OF A SOFT-SWITCHED CONVERTER FOR FUEL CELL APPLICATIONS

by

SHIJU WANG

Presented to the Faculty of the Graduate School of

The University of Texas at Arlington in Partial Fulfillment

of the Requirements

for the Degree of

MASTER OF SCIENCE IN ELECTRICAL ENGINEERING

THE UNIVERSITY OF TEXAS AT ARLINGTON

May 2006

ACKNOWLEDGEMENTS

Many people have assisted in the completion of this thesis. First, I would like to thank my supervising professor Dr. Fahimi for giving me this opportunity to conduct my research in Power Electronics and Controlled Motion Laboratory at The University of Texas - Arlington and for his continuous support during my study. The members of my thesis committee: Dr. Lee and Dr. Yeung have generously given their time and expertise to better my work. I thank them for their support and contribution. I must acknowledge as well many friends, colleagues, teachers and librarians who assisted and supported my research during my study. I am grateful to Dr. Weiping Zhang, Professor Yinru Zhang at North China University of Technology for their guidance, generous support, encouragement and deep friendship. I need to thank my friend Yashar Kenarangui for his true friendship and help. I also want to thank Yashar for spending his valuable time on revising my thesis. Thanks also to my friends Wei Jiang, Yi-der Liang, Raghunath Chellappan and members of Dr. Fahimi's lab.

I would not be where I am without endless support from my family, especially my parents, Guochen Wang, Yulan Feng and my brother, Shilong Wang and sisters, Shirong Wang, Shiqi Wang.

Finally, I would like to express my most profound love and appreciation to my dearest wife and my best friend, Liping Feng, whose patient love and endless support enabled me to complete this work. I am grateful to be able to dedicate this thesis to her.

April 11, 2006

ABSTRACT

DESIGN AND HARDWARE IMPLEMENTATION OF A SOFT-SWITCHED CONVERTER FOR FUEL CELL APPLICATIONS

Publication No. _____

Shiju Wang, M. S.

The University of Texas at Arlington, 2006

Supervising Professor: Babak Fahimi

The focus of this thesis is to design a DC-DC quasi-soft switched boost converter suitable for fuel cell applications. Study of electrical output characteristics of fuel cells was necessary for this purpose. A number of experiments were conducted to study the steady-state and transient response of fuel cell system under various load dynamics. The results of these findings were necessary for the next phase of the project which was to design a reliable and high-performance regulated DC-DC converter. The design goals were realized with a soft-switching boost converter (implementation of zero voltage switching (ZVS) and zero current switching (ZCS) schemes) that employs

a simple and effective control scheme. Key benefits of soft-switching such as high efficiency (at high switching frequencies), reduced EMI, and decreased power stress on semiconductor devices were verified. Apart from these benefits, the point that is highlighted is achieving decreased fuel cell output current ripple at higher frequencies. This is of significance because fuel cell systems prefer lower levels of current ripple which ultimately results in prolonged life time of the system. In addition, operating at high frequencies will allow for designing of high power density converters to match the high power density of fuel cells.

TABLE OF CONTENTS

ACKNOWLEDGEMENTS iii

ABSTRACT v

LIST OF FIGURES x

LIST OF TABLES xiii

CHAPTER 1

1 INTRODUCTION 1

1.1 Need for alternate sources of energy 1

1.2 Advantages and Disadvantages of Fuel cell technology 2

1.3 Challenges of integrating fuel cells with applications 6

1.4 Using new power electronics technology to enhance fuel cell application system 9

1.5 Thesis outline 11

2 OUTPUT CHARACTERISTICS OF FUEL CELL MODULE 13

2.1 Introduction 13

2.2 Fuel cell (FC) system components 14

2.3 Influence of thermodynamic variables on electrical output characteristics 15

2.4 Internal and external power losses 17

2.5 Examination of FC control module 18

2.6 Transient response of FC system 20

2.7 Experiment-obtaining steady-state and transient response 21

2.8 Experiment-output characteristics under high ripple 23

2.9 Important consideration in utilizing fuel cell models 27

2.10 Conclusion 28

3 HARD-SWITCHING BOOST CONVERTER 30

3.1 Primary considerations for modeling semiconductor devices 30

3.2 Hard switching boost converter 35

3.3 Setting up models for the semiconductor devices 36

3.4 Time varying topologies for boost converter 41

3.5 Mathematical analysis for hard-switching boost converter 45

3.6 A method to calculate duty cycle and minimum and maximum inductor currents (D, I_{L1}, I_{L2}) 53

3.7 The analytical result and hardware-test result 54

4 SOFT-SWITCHING BOOST CONVERTER 58

4.1 Introduction of soft switching technology 58

4.2 Soft switching boost converter design 59

4.3 Analysis of soft switching boost converter at different intervals 62

4.4 Obtaining duty cycle and average inductor current for power analysis 78

4.5 A method to calculate duty cycle and minimum and maximum inductor currents (D, I_{L1min}, I_{L1max}) 79

4.6 The analytical result and hardware-test result 79

5 CONTROL SYSTEM DESIGN AND HARDWARE IMPLEMATATION 84

5.1 Feedback for power electronics converters 84

5.2 Fuel cell system model 86
5.3 State-space averaging model 87
5.4 Compensator design..... 92
5.5 Hardware implementation 99
6 CONCLUSION..... 102
REFERENCES 105
BIOGRAPHICAL INFORMATION..... 109

LIST OF FIGURES

Figure Page

1.1 Experimental fuel-cell setup used for implementation and analysis 3

1.2 Block diagram illustrating the organization of a typical fuel cell system 7

2.1 Components of a typical fuel cell application 15

2.2 FC polarization curve 18

2.3 Influence of effective pressure on polarization curve..... 19

2.4 Polarization curve of the FC system from experiment 22

2.5 Toggle switch turned-on and off for various loads..... 23

2.6 Response to pulse current (ampl. 16A and freq. 1Hz)..... 24

2.7 Response to pulse current (ampl. 16A and freq. 10Hz)..... 25

2.8 Response to pulse current (ampl. 16A and freq. 100Hz)..... 25

2.9 Response to pulse current (ampl. 16A and freq. 500Hz)..... 26

2.10 Steady-state constants when load = 2.5 Ω is chopped with fuel cell system..... 27

2.11 Simplified fuel cell system model 28

3.1 MOSFET's turn-on and turn-off waveforms (case 1) 34

3.2 MOSFET's turn-on and turn-off waveforms (case 2) 34

3.3 Hard-switching boost converter..... 35

3.4 Transforming MOSFET static characterizes to dynamic characteristics 38

3.5 Typical voltage and current waveforms in diode 41

3.6 Topologies in different intervals (A: internal 1 - turning on MOSFET $0<t<t_r$; B: interval 2 - turning off diode $t_r<t<t_r+t_a$; C: interval 3 - recovering diode $t_r+t_a<t<t_r+t_a+t_b$; D: interval 4 - charging inductor $t_r+t_a+t_b<t<DT$; E: interval 5 - turning off MOSFET $DT<t<DT+t_f$; F: interval 6 - charging Cap $DT<t<DT+t_f$) 43

3.7 Diode & MOSFET operating time waveforms 44

3.8 MOSFET loss and diode loss versus frequency 55

3.9 Theoretical analysis and hardware test versus frequency 55

4.1 Boosting turn-on loss to the output 61

4.2 A. Reducing turn-off dv/dt; B. reduction of circulating current 61

4.3 Voltage and current waveforms for the switches (M1, M2, D1, D2) that indicate the operating intervals for the ideal topologies 63

4.4 Ideal equivalent circuit when M_2 and D_1 are on 65

4.5 Ideal equivalent topology when M_2 is on 67

4.6 Ideal equivalent topology when M_1 and D_2 are on 69

4.7 Ideal equivalent circuit when M_1 is on and other switches are off 72

4.8 Ideal equivalent circuit when all switches are off 74

4.9 Main diode on and ideal equivalent circuit 76

4.10 Total switching and conduction losses versus frequency 81

4.11 Efficiencies obtained from analysis and hardware tests versus frequency 81

4.12 Resonant capacitor and inductor temperature versus frequency (ambient temperature at 70 F) 83

5.1 System description of soft switching boost converter 88

5.2 Simulink block diagram for inductor current compensator with disturbance 94

5.3 Simulink block diagram for output voltage compensator with disturbance 95

5.4 Bode plot for $\frac{\widetilde{I}_{L1}(s)}{\widetilde{d}(s)}$ with integral-lead compensator 96

5.5 Inductor current response to step disturbance of 1 A 96

5.6 Bode plot for $\frac{\widetilde{v}_{C1}(s)}{\widetilde{I}_{L}(s)}$ with proportional-integral compensator 97

5.7 Output voltage small signal response to disturbance..... 97

5.8 Simulink block diagram for whole system with disturbance..... 98

5.9 System output voltage small signal response to disturbance..... 98

5.10 Hardware implementation of entire system..... 100

5.11 Soft-switching voltage/current waveforms of main MOSFET..... 101

5.12 Hard-switching voltage/current waveforms of main MOSFET 101

LIST OF TABLES

Table Page

3.1 Input current versus operating frequency (hardware test) 54

4.1 Input current versus operating frequency (hardware test) 80

CHAPTER 1

INTRODUCTION

1.1 Need for alternate sources of energy

Methods of energy production, storage and conversion have continuously been changing since the last two decades of the 20th century. Before this transient time, human livelihood demanded energy mainly from the fossil sources. But nowadays it is realized that pollution caused by these sources endanger the natural environment on which human beings and other creatures depend on. In addition, today there is a lack of certainty on the amount of the untapped reserves. On the other hand, the increase in world population and desire for high living standards demand more energy. Today there is a realization that fossil fuels have inherent limitations and the future of the societies can not depend on these for ever.

For many years, looking for new and alternate energy sources has become a challenge for every country. Some countries have addressed these challenges by utilizing alternate sources of energies like nuclear, solar, wind, tidal and other clean energy resources. The main obstacles in using nuclear energy are nuclear waste and accessibility of nuclear technology to every country. Moreover, other alternate energy sources such as the solar, wind, and tidal energies remain unrealistic when it comes to supplying the world's energy demand. It is now obvious that future of the societies is critically energy dependent. In other words, the lack of energy will be a human

catastrophe, in which it will hinder the technological advances and hence will adversely impact the quality of life. On the brighter side, engineers are developing new technologies that are leading the way towards better utilization of fossil fuels and nuclear energy, efficiency improvements in solar energy conversion, and developments in other renewable alternate energy sources. High efficiency must be considered as an important aspect in solving the possible energy crisis. In today's world, electrical form of energy is absolutely critical; however, this energy has to be converted from other sources of energy such as chemical energy of fossil source or nuclear energy. Among different sources of energy, chemical energy is viewed favorable in converting to electrical form of energy because of their abundance, and our capability to transport and store them in large amounts. There are several ways to convert this chemical energy into electricity. Although internal combustion engines are playing the main role in this area, old fashion concepts such as the fuel cells is attracting the world's attention. Starting from nineteenth century, experiments have been conducted to convert the chemical energy of fossil fuels directly into electricity.[1] High efficiency and non-polluting nature of the fuel cell systems make them one of the potential candidates for our future energy solution.

1.2 Advantages and Disadvantages of Fuel cell technology

Figure-1.1 shows a proton-exchange-membrane (PEM) fuel cell stack and its hydrogen tanker, and the whole system is located in Power Electronics and Controlled Motion Laboratory at University of Texas- Arlington.

Figure-1.1 Experimental fuel-cell setup used for implementation and analysis

A fuel cell is an electrochemical device, and produces electricity by utilizing an electrochemical reaction to combine hydrogen ions with oxygen atoms. A typical PEM fuel cell includes an anode, a cathode, proton exchange membrane (which blocks electrons), and catalysts (which facilitates the reaction of oxygen and hydrogen). Pressurized hydrogen gas (H_2) enters the fuel cell on the anode side. When an H_2 comes in contact with the catalyst, it splits into two H^+ ions and two electrons (e^-). The electrons pass through the external circuits to do electrical work, and get in touch with the cathode side of the fuel cell. Meanwhile, on the cathode, O_2 forms two oxygen atoms under the catalyst. Each of oxygen atoms combines with two electrons to form

O^{2-} ion which attracts the two H^{+} ions through the membrane, where they react to generate water molecule (H_2O).[2,3]

Some major advantages of fuel cell systems which make them attractive contenders in many applications are:

a. Unparalleled environmental performance – the conventional generation of electricity produces more particulates, Sulfur Oxides and, Nitrogen Oxides than all other stationary industrial sources combined.[4] A PEM fuel cell stack itself operates on hydrogen, thus, water is the only by-product from the stack reaction. Besides minimizing emissions of regulated pollutants, a fuel cell system is also relatively quiet which makes its overall impact on the environment minimal.

b. High efficiency – the system is nearly double the simple-cycle efficiency of conventional gas turbine and reciprocating engine power generation technologies. Due to the ability to integrate power production in dwelling areas, efficient use of the waste heat is possible. Another feature of fuel cells is the similarity between the efficiencies of small systems and large ones.[5,6]

c. Continuous output – a fuel cell is similar to a battery. The advantage of fuel cells over batteries is their ability to continuously produce electrical output through replenishing their reactants (hydrogen and oxygen). In other words, fuel cells produce electricity from an external fuel supply as opposed to the limited stored energy of batteries.

d. Fuel diversification – this technology uses hydrogen which can be made not only from fossil fuel sources but also from biomass and some other alternate sources.[8]

e. Durability and maintainability – a mature unit is typically designed to function for up to 20 years and operates for about 40,000 hrs between overhauls.[5, 6]

f. Reliability and flexibility – fuel cells contain very few moving parts; therefore these systems have much higher reliability than combustion engines, turbines or combined-cycle systems. Because of the less number of rotating parts, fuel cell systems will not be prone to various breakdowns, unlike combustion engine systems; this also makes fuel cell systems inherently silent.

g. High power density – new technologies in material science and novel fuel delivery mechanisms have allowed power density of fuel cells to exceed that of lithium ion (Li-ion) batteries.[7]

h. Wide ranges of applications – fuel cells have a variety long ranging potential applications. Environmental considerations are increasing worldwide, so utilities are increasingly forced to deal with the trade-offs between power generation and the associated environmental consequences. Because of the environmental concerns, fuel cells can also be an attractive choice for the transportation industry. On the other hand, the market for very low power applications (around 1-5W) has more potential when considering relatively high costs, weight and power density of batteries.

However besides many advantages of fuel cells that some were mentioned above, these systems also pose new challenges that need to be overcome before they can be fully utilized.[8] Some of the disadvantages of fuel cells are:

a. High cost – catalysts (such as platinum) are relatively expensive. The cost of hydrogen equipment, other components, manufacture difficulties and additional auxiliary devices (converters and inverters) are also high.
b. Short lifetime – experimental fuel cell system shown in Figure-1.1 only has 1500-hour life time.[9]
c. Wide fluctuating low dc-output-voltage – the experimental fuel cell system shown in Figure-1.1 outputs 22-50V unregulated DC voltage.[9] This kind of output characteristic is incompatible with most devices and appliances powered by the existing utility system
d. Slow dynamic responses under sudden load changes – mechanical components are involved in fuel cell operation. Consequently, a conversion device having fast dynamic response is necessary as part of a fuel cell application.
e. Relatively long startup process – the experimental fuel cell system shown in Figure-1.1 needs 2 minute to achieve rated power from a cold start condition.[9]

1.3 Challenges of integrating fuel cells with applications

A typical structure of a fuel cell system for a power application is illustrated in Figure-1.2. It comprises of a fuel cell stack as the primary source, a dc/dc converter to obtain utility level dc voltage, and a dc/ac inverter to obtain isolated ac voltage (which

is compatible with the existing utility system). In addition, most of today's electronic devices are compatible with utility level dc voltage and they can be directly powered by utility level dc voltage. The current utility system only provides an ac voltage source whereas most of the electric devices and appliances require dc voltage for their operation. This leads to the integration of rectifiers to electric devices and appliances, thus increasing complexity and cost. On the other hand, fuel cell systems provide not only ac power but also dc power to eliminate the need of a rectifier, and thereby this reduces cost and complexity of the systems.

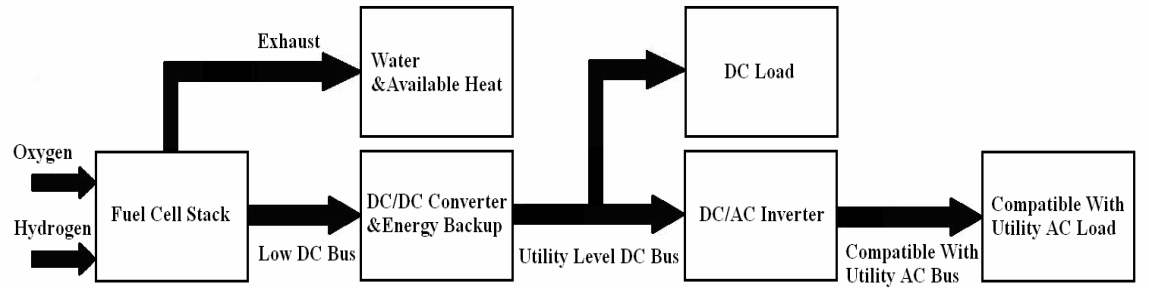

Figure-1.2 Block diagram illustrating the organization of a typical fuel cell system

The fuel cell shown in Figure-1.1 produces low dc voltage (22 ~ 50V). Most adjustable speed motor drives and appliances require utility level dc voltage (120V) or ac voltage to operate. Therefore a converter is required in order to transform the low dc output voltage of fuel cells to a desirable high dc voltage. A typical fuel cell based power converter has two parts: First part is a dc/dc converter, which converts the variable low dc output voltage of the fuel cells to a regulated high dc voltage; the

second part consists of either a battery or an ultra capacitor as an energy storage backup in order to improve load dynamic response.

To design a cost-effective and highly efficient dc-dc converter, a proper topology is selected to be suitable with fuel cell characteristics. Among many solutions, no one stands out as the clear winner. Compromises should be made in considering size, efficiency, input voltage range, and other parameters when selecting a converter topology. Below is a list of some general topologies:

a. Inverter with step-up voltage transformer
b. Forward converter with step-up transformer
c. Cuk converter
d. Boost converter

Other possibilities include buck-boost converter and various isolated topologies such as half-wave inverter, but they are either too similar to the above topologies or too complex to be more efficient and reliable for fuel cell systems.

The pros and cons of the above suggested topologies will be discussed and the reasons will be provided for the final selection. The listed inverter topology seems to be an obvious first choice for the purpose of stepping-up voltage. This system consists of a transformer and more than two semiconductor devices. Because of the number of semiconductor devices, its inadequate reliability, high cost, and poor efficiency, this is not a proper solution. Also this topology draws current in pulses which due to the slow dynamic response of fuel cells it is a major draw back. The simplest of big power transformer-isolated topologies is the forward converter, whose simple switching circuit

requires only one power semiconductor in the low voltage side. Even though this topology only has a single magnetic core, it has the problem of dc magnetization. This topology also suffers from requiring pulse input current just like the inverter topology. When considering the Cuk converter, although this topology does not draw pulse current, it requires too many energy-storage elements, and hence is not an attractive candidate for this application. Finally we consider the Boost topology which at first glance seems a good choice due to its simplicity. Moreover, because of the series connection of the power source (fuel cells) and the inductor, boost converter draws continuous current from the source. This is important because drawing continuous current suits the dynamic characteristic of fuel cells; this also sufficiently utilizes fuel cells' output capability. In conclusion, boost converter is a simple power circuits in which low cost, high efficiency and high reliability can be achieved. Therefore, this appears to be the best choice for fuel cell applications amongst all the listed topologies.

1.4 Using new power electronics technology to enhance fuel cell application system

In the past two decades, there has been a rapid development in the area of power electronics; however, new switching power supplies have to be developed in response of the modern needs of the electrical industry. Some of these include very high conversion efficiency, high power density, elimination of EMI and RFI emissions, fast dynamic system response and, elimination of undesired harmonics which cause problem to the utility system.

To address some of the shortcomings of traditional converters, new power electronics circuits are being designed based on resonant and soft switching technologies. A resonant converter uses semiconductor components and resonant L-C circuits to 'naturally' change current routes instead of only using semiconductor components to force currents to change their flowing loops. In other words, L-C circuits cause voltages/currents in semiconductor switches to cross zero as the semiconductor switches are turned on or turned off. This will allow the realization of nearly zero switching losses while a converter switches between different modes. All resonant converters essentially use the same concept, which is to provide a lead or lag between the current and the voltage in a semiconductor device. This phase difference will prevent the voltage and the current to be present concurrently in a semiconductor device. Although this concept seems simple at first, there exits a variety of possible topologies, that can be implemented to realize resonant operation. Even though introducing resonant technology enhances a converter's performance, it comes at a price of adding complexity.

Two of the most important advantages of fuel cells are their high efficiency and high power density. In designing the converter, these factors must be considered. Although hard switching boost converter has relatively acceptable efficiency and power density, it has unacceptable EMI and RFI. In order to overcome these setbacks in the hard switching boost converters, it is worthwhile to consider implementing resonant technology in these converters.

A resonant boost converter is reported to have improved efficiency of converter systems by reducing switching losses. This is realized by implementing zero-voltage-switch (ZVS) or zero current switch (ZCS) schemes. Reducing switching losses in such a manner will enable the converter to operate at high frequencies. With the increase in frequency, smaller values of inductors and capacitors will be possible, which allow for the reduction in component sizes. The reduction in sizes of these components will further increase the converter power density. Also because of smaller values for energy storage devices, smaller time constants are achieved, which provide the converter with a faster dynamic response. This system also reduces EMI and RFI through the benefits of ZVS and ZCS technology. Finally, with the implementation of a simple control system, overall cost of the converter, along with its reliability, can be improved.

1.5 Thesis outline

Brief reasons for selecting a boost topology were given in section-1.3. Experimental results reported in this thesis as based on soft switching and hard switching boost converters that were designed and built in the UTA/PECM lab. In Chapter-2 the output characteristics of fuel cell systems are examined and experimental results from extensive tests are reported. This information can help in developing a fuel cell system model when designing a power electronics module. In Chapter-3 a method is introduced for the calculation of power losses for a hard switching boost converter. Then these results are compared against experimental measurements from the hard switching boost converter. In Chapter-4 the same objectives were pursued as Chapter-

3, but this time for a soft switching boost converter. Then a detailed comparison of soft switching and hard switching efficiencies is presented. In Chapter-5 small-signal linearization of state-space averaging model is established for the purpose of frequency-domain control design. Then a simple and effective control scheme for quasi-boost converter is presented. Main points of this thesis are summarized in the conclusion.

CHAPTER 2

OUTPUT CHARACTERISTICS OF FUEL CELL MODULE

2.1 Introduction

A fuel cell application involves ideas from diverse disciplines such as chemistry, electronics, material science and fluid control. Main aspect of a fuel cell is an electrochemical reaction that produces electricity with water and heat as byproducts. Fuel cells have numerous outstanding characteristics that make them attractive for several crucial applications such as transportation, power generation, and portable devices. Some of the prominent features of these energy conversion devices include environmentally friendly emission and high efficiency compared to combustion engines.[10] Today many companies including almost the entire automotive industries have invested stake in fuel fell technology. This represents a variety of fuel cell (FC) technologies that currently are being developed towards various applications and thus require different operating specifications.[11] Power electronics has the vital task of interfacing the clean and efficient energy from fuel cells to diverse spectrum of applications. Even though FC systems are extensive and complex devices, a power electronics engineer is mainly interested in their electric output characteristics for design of an appropriate power electronics module in order to meet the load specifications. In this chapter the role of control module in FC system is discussed. Moreover, it is shown how the control module modifies steady state and transient

electrical output characteristics of FC stack. The fuel cell module as an example discussed here is Ballard Nexa™ 1.2kW proton exchange membrane fuel cell system, which consists of its necessary interfaces and air-cooled fuel-cell stack. Experimental results are presented to verify arguments presented based on fuel cell models. Then based on the results of these findings, acceptable types of power electronics circuits for FC applications are recommended and the utility of ultracapacitor is emphasized in applications involving faster dynamics.

2.2 Fuel cell (FC) system components

The experiments were conducted by utilizing a Ballard Proton Exchange Membrane (PEM) fuel cell (Nexa™ 1.2 KW DC Power Module). The device ratings are as follows: rated net power: 1200 watts, rated current: 46 Amps, DC voltage range: 22 to 50 Volts.[12] PEM fuel cell is one of the most widely studied types of fuel cells and its primary performance characteristics match those of other fuel cell types.[10] One example of complete FC applications, represented in Figure-2.1 block diagram, involves ideas from diverse disciplines such as chemistry, material science, mechanical engineering, and electrical engineering. FC system, Figure-2.1, (block-C) consists of FC stack (block-B), a control module (block-C), and other auxiliary devices (e.g., compressors, valves). FC stack is the core of this system where the energy conversion takes place. Inside each fuel cell, chemical energy of hydrogen molecule is directly converter to electrical energy by means of electrochemical reaction. In order for any chemical reactions to result in the desired outcome, specific pressure, and temperatures,

along with right amounts of reactants need to be provided. Therefore additional equipment is necessary to support Nexa™ system's operation; that is to provide pressurized air (compressor/air pump) and regulate reaction temperature (cooling fan). Also control module is utilized to optimize the operation of FC system (sensors, actuators and controllers). Auxiliary equipments consume power for their operation and as a result introduce losses that reduce the total efficiency of the system.[12] It will be shown in the following paragraphs how the utility of a control module (comprised of electrical, mechanical elements) can reduce the inefficiencies posed by the energy conversion operation and by auxiliary equipments.

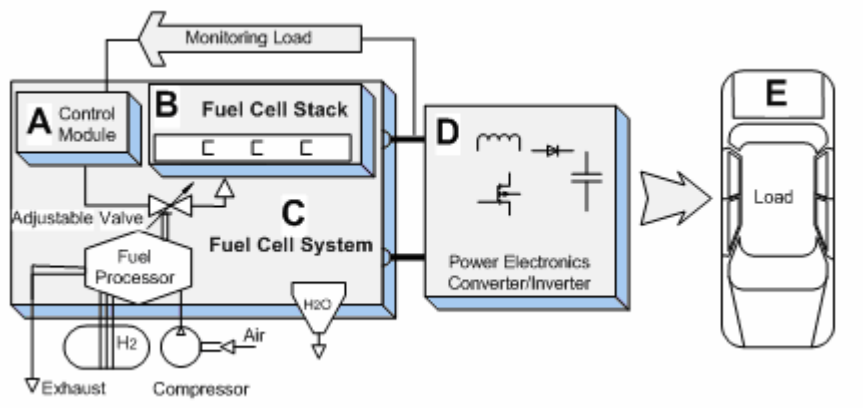

Figure-2.1 Components of a typical fuel cell application

2.3 Influence of thermodynamic variables on electrical output characteristics

In order to effectively utilize the energy stored in hydrogen molecules, mathematical equations are necessary to express voltages and currents in terms of variables involved in electrochemical reactions. Mathematical equations developed for this purpose are highly complex while too many variables are involved in the process of

energy conversion. However, appropriate assumptions are made in many sources in order to drive approximate expressions for the variable of interest. It is of interest to express the output stack voltage of FC in terms of other chemical, thermodynamic, electrical variables:[13]

$$V_{stack} = f(I, P_{O_2}, P_{H_2}, T_{FC}) \tag{2.1}$$

The following equation is derived from Nernst and Tafel equations with appropriate approximations to simplify the result. The assumptions of this model are as follows: insignificant anodic activation voltage, insignificant water hydration, uniform current density, and uniform temperature.[14,15,16]

$$V_{stack} = n \times E_{cell}$$

$$V_{stack} = n\left\{ \underbrace{E_0 + \frac{RT}{2F}\ln\left(p^*_{H_2} \cdot \sqrt{p^*_{O_2}}\right)}_{INTERNAL-VOLTAGE} - \underbrace{\frac{RT}{2F}\ln\left(\frac{I}{I_0 \cdot p^*_{O_2}}\right)}_{OVERPOTENTIAL-VOLTAGE-DROP} - \underbrace{\frac{I \cdot t_m}{\delta}}_{OHMIC-VOLTAGE-DROP} \right\} \tag{2.2}$$

V_{stack} : FC stack voltage or output terminal voltage

E_{cell} : FC voltage

E_0 : Open circuit potential

$\boldsymbol{n}$: Number of cells in FC stack

T_{FC} : Temperature in kelvin of FC channel [K]

$p_{H_2}^*$: Effective partial pressure of hydrogen

$p_{O_2}^*$: Effective partial pressures of oxygen

I : FC stack current or load current

I_0 : Exchange current density [A/cm^2]

R : Ideal gas constant [$8.3143 J/(mol \cdot K)$]

δ : Electrolyte conductivity

t_m : Thickness of FC membrane

* : Indicates effective value

2.4 Internal and external power losses

Equation-2.2 can be used to develop a voltage/current curve such as the one shown in Figure-2.2. This curve, also called polarization curve, is important in characterizing the operating point of FC stack. Steady-state voltage/current values in each region of the curve are affected by particular dominant losses.[10] At normal loads, the curve is characterized by an almost linear region, where the voltage drops are due to second and third terms of Equation-2.2. At heavy loads, I has a higher value, while $p_{O_2}^* \cdot I_0$ remains unchanged, which explains the sharp dive of the curve at heavy loads.

FC voltage consists of three parts: internal voltage, voltage drop due to overpotential, and voltage drop due to resistance of membrane.[10] From Equation-2.2, the load current and effective partial pressures of hydrogen and oxygen determine how

stack voltage varies. Increasing $p_{O_2}^*$ and $p_{H_2}^*$, increases internal voltage and thereby enhances the output voltage. Also increasing $p_{O_2}^*$ reduces overpotential voltage drop and further enhances the output voltage. On the contrary, increase in load current has a deteriorating effect on the output voltage since it increases both the overpotential and the ohmic voltage drops. Overpotential and ohmic losses can be considered as the internal losses of the system, whereas, losses due to power consumption in air pump, cooling fan, and control circuitry are the external losses. At rated system power, external losses reach approximately 250 watts.[12] Control circuitry involves only signal level voltages and currents, thus does not consume significant amounts of power; however the cooling fan can consume power in range of 20-40W. This implies that power consumed by the air pump for the most part is responsible for the external losses.

2.5 Examination of FC control module

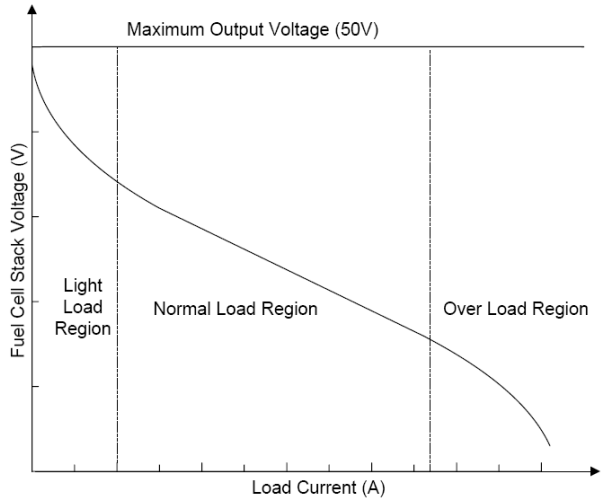

Figure-2.2 FC polarization curve[10]

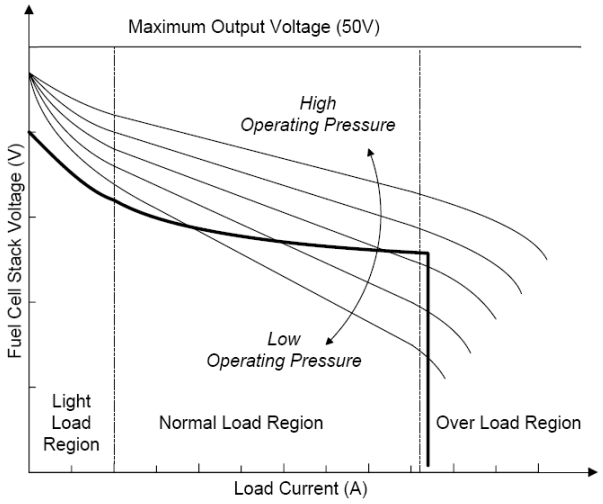

Figure-2.3 Influence of effective pressure on polarization curve[12]

As shown in Figure-2.3, increasing flow rate of oxygen ($p_{O_2}^*$) causes the polarization curve to become less steep which is confirmed by Equastion-2.2. This results in lower internal losses but unfortunately it will lead to higher external losses and higher mechanical stresses in flow-field-plates.[12] This is because the air pump has to invest more power to increase the airflow. The basic function of the control module is summarized in the following way. At light loads, where output current is low, external losses are dominant. Therefore, to enhance efficiency at light loads, air pump is operated at low speeds to prevent unnecessary losses. On the other hand, at normal loads, where output current is high, internal losses are dominant. Also at normal load, where output power is high, system can afford more external losses in order to prevent too much overpotential losses. As evident from Equation-2.2 and Figure-2.3, this is done by increasing the flow rate of oxygen ($p_{O_2}^*$) in order to reduce overpotention

voltage drop. This will raise the curve in Figure-2.3 and reduce the overpotential losses. Even though, the process of increasing the flow rate of O_2 leads to increased external losses, the overall efficiency of the system is improved. As shown in Figure-2.3, bolded-line represents the steady-state of the system with addition of a control module. Comparing this to other curves indicates that the controller prevents the output voltage from declining too fast. This highlights the distinction between output characteristics of FC stack with and without the control module. Eventually at some point, the load current becomes very high, while air pump reaches its limit; at this point the controller will shut down the system. Unfortunately, the ohmic losses can not be improved in this way. In summery, the main task of FC control module is to make a compromise between higher external losses and much improved internal losses in order to enhance the overall efficiency of the system.

2.6 Transient response of FC system

The above discussion only concerns the steady-state response of FC system. The analysis of transient responses is more complex since it can not easily be expressed by an equation. Fuel cells exhibit poor transient responses and suffer dynamic limitations. Transients occur in both current and voltage and their intensity (overshoot and oscillation) is proportional to magnitude of load current steps.[17] The main problem is the slow dynamics of FC system in tracking the load demands. This is mainly due to mechanical constrains in transporting and utilizing the necessary reactants rather than the speed of electrochemical reaction itself. Sharp increase in load transport of reactant

gases is not able to catch up to the reaction demand and therefore voltage suffers a sharp dive.[13] This brings about reaction starvation and can cause fuel cells to fail. Another task of a controller is to shut down the system before a permanent damage can occur in this way.

Usually due to the proprietary classifications, exact functionality of control-modules is not specified in the manuals of FC manufacturers. Even though studies (such as the one demonstrated above) can be helpful in providing insights into how FC systems behave, the exact electrical response (steady-state and transient) of the system to load variations is not clear. This imposes an additional obstacle to a power electronics circuit designer. Before investing in the actual design of a power electronics circuit and/or controller, a number of experiments need to be performed to gain a sufficient knowledge regarding the response of FC system in hand to variations in loads.

2.7 Experiment-obtaining steady-state and transient response

Experiments were conducted that verify the results from the above analysis. The objective of these experiments was to develop number of tests to extract information about the steady state and transient output characteristics of the FC system in hand. First the output terminal of FC system was connected to resistors in range of 0.7-66.5 ohms using a toggle switch. In this way, the actual polarization curve of the system was obtained that describes the voltage and current variation at the output terminal, shown in Figure-2.4. In order to obtain information about the transient response of FC system, the resistors were suddenly connected to the output terminal and

thereby impulsive changes in load current were produced. The settling time of the transients represent the time it takes for the terminal voltage to reach steady-state; from data it is a function of load current, shown in Figure-2.5. We note that as load current increases, the transient response noticeably improves. The short rise-time at higher loads can be due to the fact that the flow rate of O_2 is already high in the flow-field-plates and therefore the reaction is able to quickly reach the no-load-voltage (maximum voltage). The short settle-time at higher loads can be due to smaller time constant of FC stack (RC, R: load, C: internal capacitance of stack) since higher load current implies lower load resistance. It is concluded that the flow rate is unable to quickly respond to variation in load current.

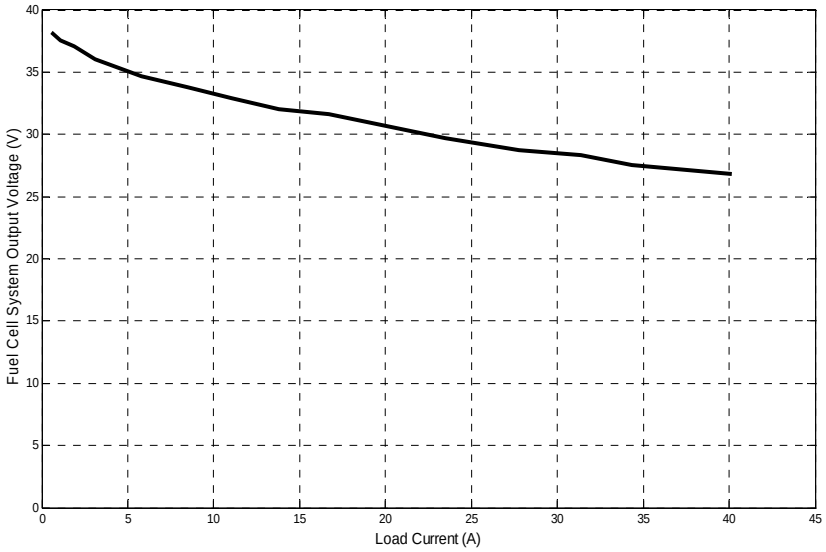

Figure-2.4 Polarization curve of the FC system from experiment

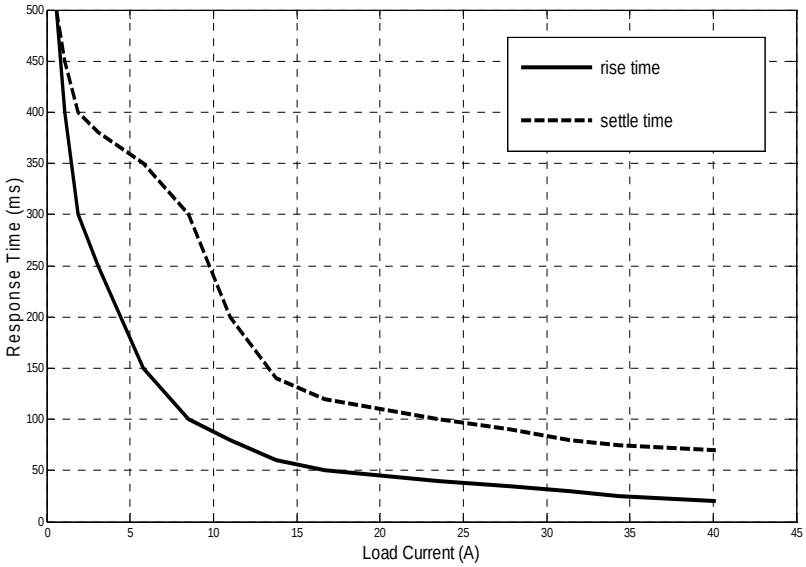

Figure-2.5 Toggle switch turned-on and off for various loads

2.8 Experiment-output characteristics under high ripple

Next a chopper with a resistor load was placed at the output of FC system and response was noted, shown in Figure-2.3-to-2.6. The effect of internal capacitance of FC stack is apparent from these figures. From Figure-2.6, it is seen that the current initially rises to charge the internal capacitor then settles at a steady-state voltage. From Figure-2.7 and -2.8 it is seen that there is not enough time for capacitor to charge and therefore does not reach steady-state voltage. Based on this, FC system is not able to respond well to frequencies as low as 10 Hz. In addition, audible noise is produced for frequencies above 100 Hz that point out to the presence of mechanical stress that can shorten the life time of the system. A buck converter is not recommended to be connected directly to FC system since it demands the same type of current as the chopper. Instead, a boost converter which draws an almost constant current from the

source is suitable for FC applications. We conclude that even though FC control module improves the steady-state response of FC stack, it does not improve the transient response. As mentioned before, this is because of long time constants of pumps and valves. It also takes some time for the reactant gases to travel through the channels. Relatively slow mechanical components of the system can not respond fast to control signals and therefore are unable to track fast changes in the load. In applications such as electric vehicles that entail fast load dynamics, ultracapacitors are utilized as auxiliary power source to supply the transient energy demands.[18,19]

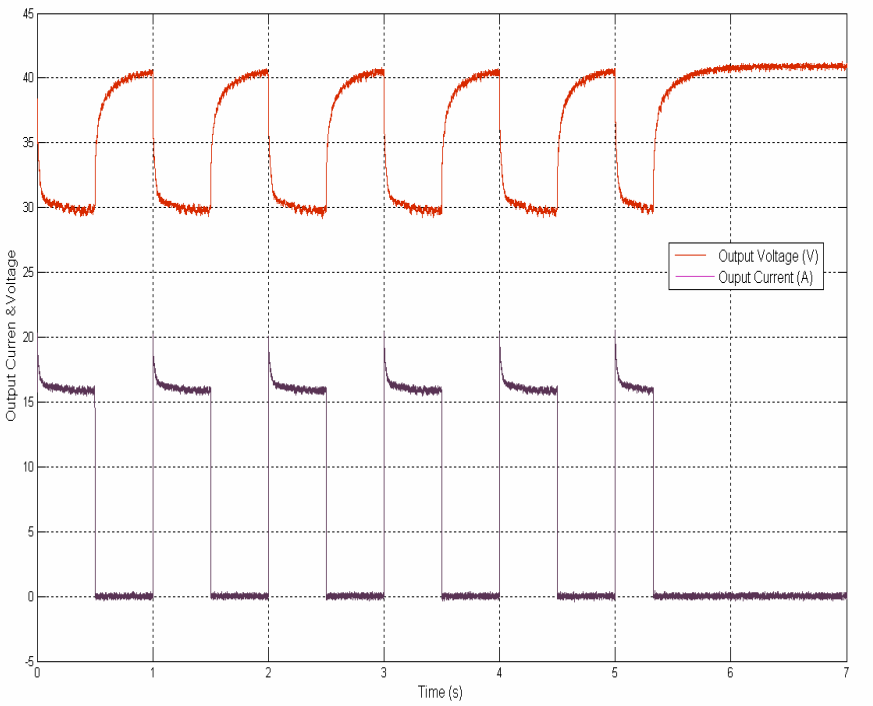

Figure-2.6 Response to pulse current (ampl. 16A and freq. 1Hz)

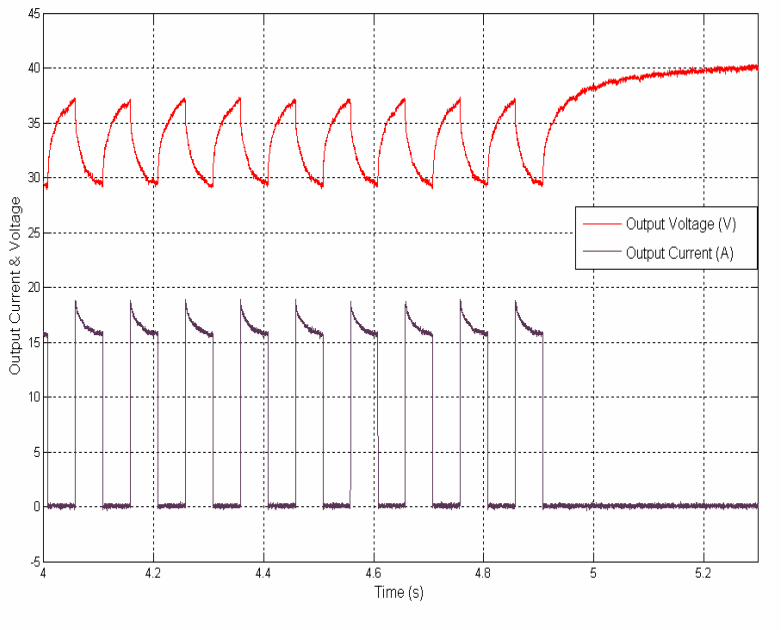

Figure-2.7 Response to pulse current (ampl. 16A and freq. 10Hz)

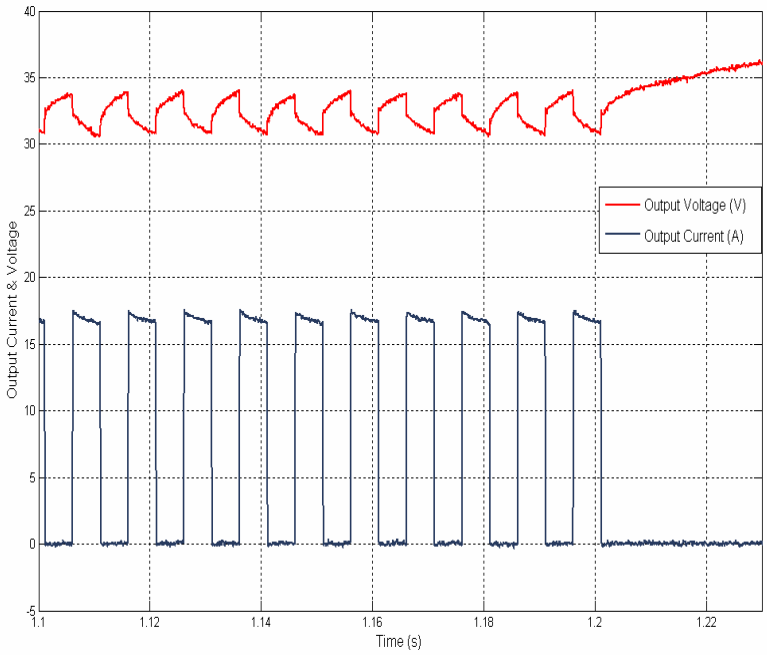

Figure-2.8 Response to pulse current (ampl. 16A and freq. 100Hz)

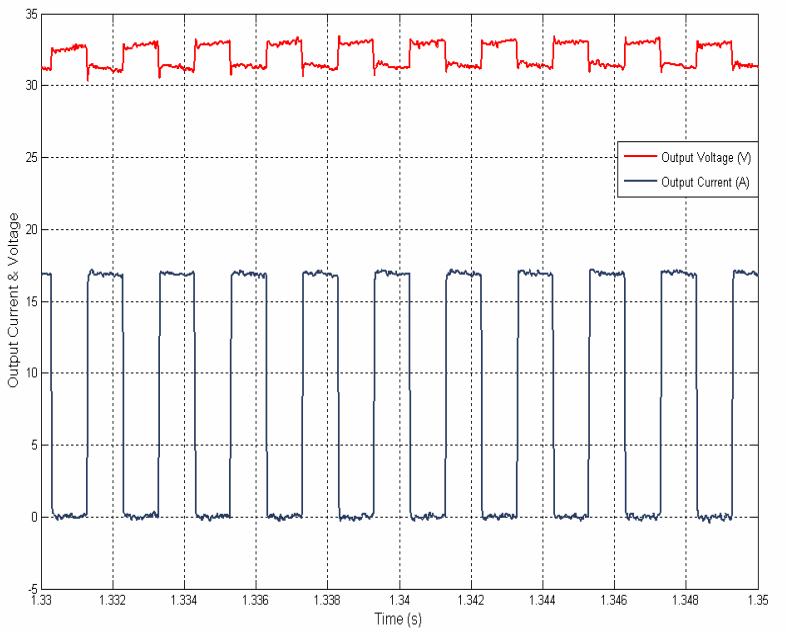

Figure-2.9 Response to pulse current (ampl. 16A and freq. 500Hz)

Next, rising and falling time constants were calculated. It was found that the time constant is a function of output current frequency. As shown in Figure-2.10, time constant goes to zero as frequency increases. This is also evident from Figure-2.9 in which the time constant appears to be zero at 500 Hz. In the next section, this result will be used in developing a model for fuel cell system.

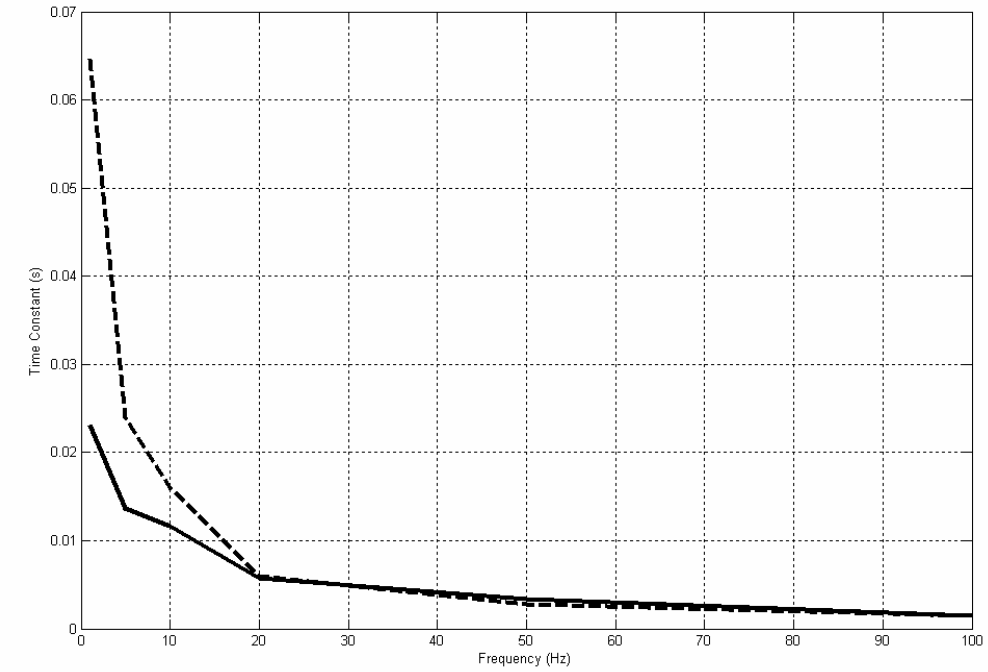

Figure-2.10 Steady-state constants when load = 2.5 Ω is chopped with fuel cell system

2.9 Important consideration in utilizing fuel cell models

An appropriate fuel cell model is necessary in order to design a reliable and high performance converter for a fuel cell application. There are different models that have been developed for fuel cell systems. A model needs to be developed with considering the specific application in hand. We can conclude from the above discussion that the fuel cell system prefers a steady output current. Any fast dynamics of the current will result in mechanical stresses of the system and will shorten the lifetime of the fuel cell. Also fuel cell system is unable to supply fast power demands of the load. This means that in a fuel cell application, energy backup elements of the converter system are responsible for transient energy delivery and transient energy recovery. In designing a

control system for the converter it is necessary to confine the output current of the fuel cell system (input current of the converter) to low frequencies. With the assumption that the control meets this requirement a fuel cell model such as the one shown in Figure-2.11 can be utilized. There are two important considerations in this model. First, by deliberately making the controller current loop sluggish, steady current is obtained at the output that results in a negligible capacitor effect. Secondly, at high frequency currents, such as current ripple caused by switching action, rising and falling time constants appear to be zero and therefore transients are not observed at the output, as illustrated in Figure-2.9. With these assumptions, a fuel cell system model shown in Figure-2.11 can be utilized.

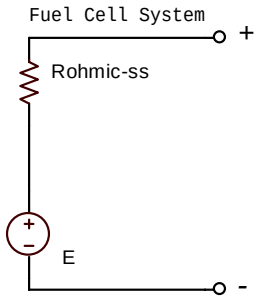

Figure-2.11 Simplified fuel cell system model

2.10 Conclusion

Based on experiments presented in this chapter, FC control module used here improves the steady state response of the FC system. In addition, FC control module has inherent short comings in responding to the transient load demands. Design of a power electronics converter/inverter for FC application requires special attention to the

ripple and frequency in order to avoid unexpected input to the converter/inverter circuit and also to prolong the life-time of FC system.

CHAPTER 3

HARD-SWITCHING BOOST CONVERTER

3.1 Primary considerations for modeling semiconductor devices

Today size, weight, and acoustic noise (caused by the cooling system) are some of the challenges in designing new power electronic converters. In order to address these challenges, a converter has to be able to operate efficiently at higher frequencies, meaning, switching losses should be as minimal as possible during one switching period. At a specific frequency, some of the losses in semiconductor components can be improved based on the design, unlike losses in other components. In analyzing power electronic circuits operated at high frequencies, it will not be sufficient to simplistically model semiconductor devices as ideal switches (no losses with zero turn on and off times). Therefore, employing a suitable model for diverse power electronic applications becomes important.

Every semiconductor manufacturer provides datasheets with very detailed explanations of their devices, but a power electronics designer only needs to extract certain information that is needed for his/her design application. Therefore designers need to understand which characteristics of semiconductor devices would mainly affect the operation of a power electronic circuit. A semiconductor device in a power electronics converter is desired to operate in two regions: saturation and cutoff; however, the commutation regions can not be avoided and therefore have to be taken

into consideration. Commutation is a transient region between the saturation and cutoff regions that occurs when the device turns on and off. Certain assumptions and considerations have to be made when a device operates in each respective region. When operating in the cutoff region, breakdown voltage becomes an extremely important consideration, since exceeding this value will cause the circuit to malfunction and even can damage the device. Another factor that influences the losses in these circuits is the leakage current. Even though the manufacturers try to minimize this current as much as possible, the power electronics designers have no control over this. In the saturation region, main considerations are the maximum conducting current, the forward voltage drop (diode), the equivalent resistance (MOSFET). In some applications maximum pulsed current also has to be considered for this region. In the commutation regions (turn on and off), switching times determine the maximum frequency at which a semiconductor device is able to operate. Specifications that were mentioned, influence the losses, determine the operating temperature, and also set the boundaries for the proper operation of a semiconductor device.

Power losses at high frequencies are the main bottle neck in designing smaller size converters for a certain power level. From the above discussion, the power losses in a converter are influenced by various factors such as semiconductor device characteristics. Nevertheless these losses are not limited to device characteristics, and are also greatly influenced by the choice of topology. The power losses in semiconductor devices can be classified as two types: conduction losses which occur in the saturation and the cutoff regions, and switching losses which occur in the

commutation regions. The following discussion will consider the main factors which influence power losses in each of the operating regions, namely cutoff, saturation, and commutation regions.

1. Power loss in the cutoff region: in this region the power loss is caused by the leakage current and the voltage across a semiconductor device. The leakage current is very small in modern silicon devices, and therefore this power loss can be neglected. If a more detailed model of a semiconductor device is needed, it can be modeled as an equivalent resistor in this region. The value of this equivalent resistor is obtained from the value of leakage current at the voltage specified in the data sheet.
2. Power loss in the saturation region: in this region the power loss is caused by the current through the device and the forward voltage across it. Device characteristics and the current will determine the magnitude of this loss. Therefore the current is the major consideration for low frequency operation. In the analysis of power electronics circuits, an equivalent small voltage source or small resistor is used to model a semiconductor device that is operated in this region.
3. Power losses in the commutation regions: a semiconductor device has two commutation regions, one is when the device goes from cutoff to saturation region and the other is when the device goes from saturation to cutoff region. In the first region (turning on), there is a period of time in which voltage and current exist simultaneously. As shown in Figure-3.1 and Figure-3.2, there are

two cases for this transition, depending on the choice of topology. As shown in Figure-3.1, in the first case, the current starts rising as the voltage starts to drop (interval t_r). In the second case, shown in Figure-3.2, the current starts rising even though the voltage is still fixed at the cutoff region (t_r). Then the current must rise to the peripheral current before the voltage starts to drop (t_a). In the second commutation region (turning off), the current starts to drop as the voltage starts to rise, and then they reach their final values simultaneously (t_f). The simultaneous presences of voltage and current in the device cause considerable power loss. Therefore, turn-on and turn-off times become particularly important when employing hard switching. This sets an inevitable restriction in increasing the frequency of operation in hard switching applications. Even though there are methods to increase the switching speed to some degree, this only provides a limited room to increase the frequency. It should also be noted that electromagnetic interference (EMI) is the downside to faster switching. This means that Electromagnetic Compatibility (EMC) is another obstacle in hard-switching application design. As the switching period is reduced through the use of improved driving circuits, faster rise and fall times are obtained which in turn generates higher frequency noise. This noise is emitted and transmitted out of a converter. Therefore there needs to be a compromise between efficiency and EMC. Another limiting factor for high frequency operation is the thermal effect and the power stress which can impact the lifespan of semiconductor devices. Therefore, proper design of hard switching converters is a compromise

between several objectives such as increasing the efficiency, reducing the size, increasing the semiconductor's lifespan, and meeting EMC.

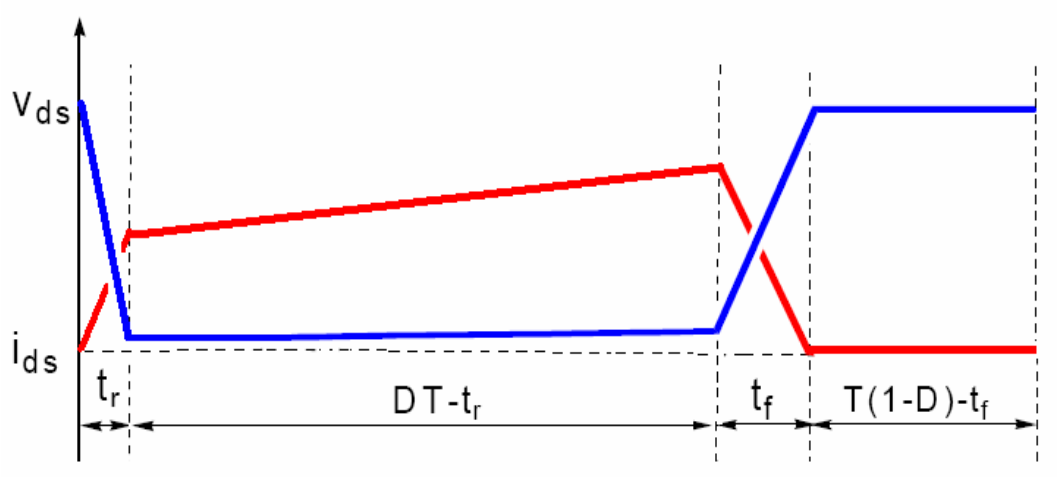

Figure-3.1 MOSFET's turn-on and turn-off waveforms (case 1)

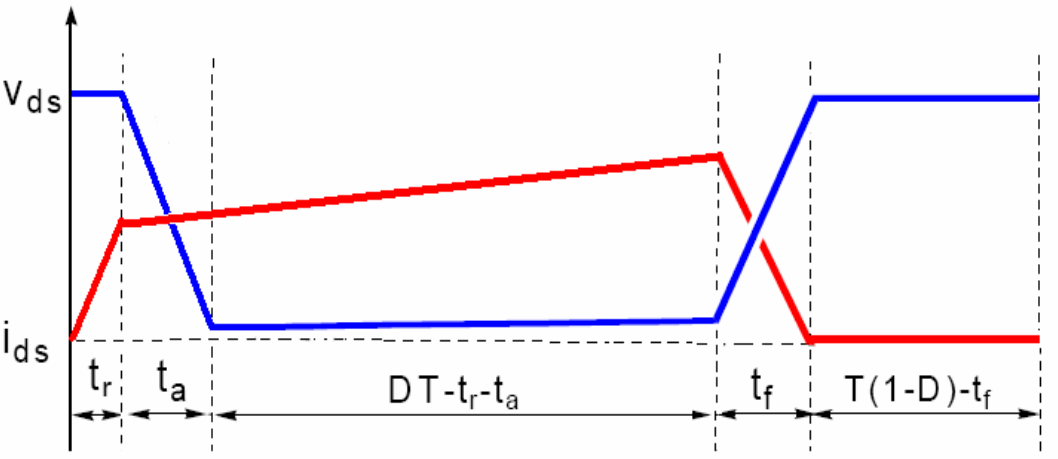

Figure-3.2 MOSFET's turn-on and turn-off waveforms (case 2)

3.2 Hard switching boost converter

As mentioned already in Chapter-1, the fuel cells generate a fluctuating low-DC voltage which is not suitable to use in general applications which use the existing utility system or automotive appliances. A typical power electronics converter, hereof the boost converter, is used in order to facilitate DC transformation. When fuel cell is connected as the input to this converter, it will yield an output which is greater than the input voltage

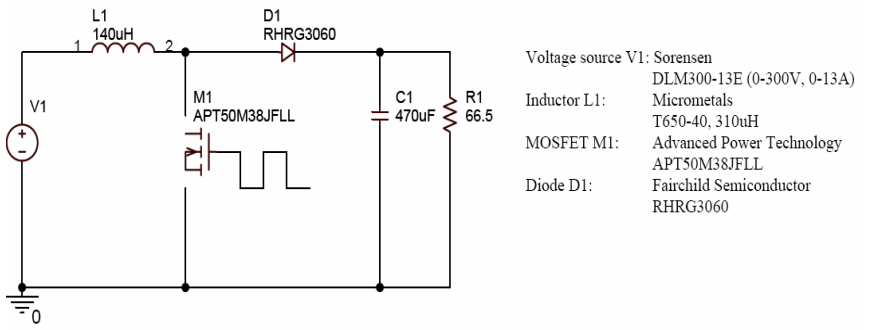

Figure-3.3 Hard-switching boost converter

A boost converter is shown in Figure-3.3 with a fluctuating input voltage of 22-60V and a regulated output voltage of 200V (1±1 %). This topology has two non-linear semiconductor devices. To analyze this circuit, understanding the physics of these devices is not necessary and a power electronics designer only needs to consider the circuit models in order to conduct a reasonably accurate analysis of the circuit. Models are necessary in order to perform a variety of analysis such as the calculation and estimation of losses, efficiency, junction temperature, and device power stresses,

thereby enabling the designer to make correct decisions to optimize the design. Next we will consider and setup adequate models for the MOSFET and diode from the application side.

3.3 Setting up models for the semiconductor devices

1. Cutoff region: In this region both the MOSFET and the diode can be modeled as resistors. The values for these resistors are obtained by considering the worst case scenario when the junction temperature is at 125°C. When the gate voltage is $V_{GS} = 0V$, the drain voltage is $V_{DS} = 400V$ and, the drain leakage current is $I_{DSS} = 1000uA$,[20] it is calculated that the equivalent resistance is $R_{DSS} = 400k\Omega$. In the case of the diode, when reverse voltage is $V_{RM} = 400V$ and reverse leakage current is $I_R = 1000uA$,[21] it is calculated that the reverse equivalent resistance is $R_R = 400k\Omega$. Due to the high values of these resistances, these devices are considered open circuits when operated in these regions.
2. Saturation region: In this region the MOSFET is modeled as a small resistor and the diode can be models as a small dc-voltage source. The value for this resistor is obtained by considering the worst case scenario when the junction temperature is at 125°C. When the gate voltage is $20V \geq V_{GS} \geq 10V$, it can be obtained from the datasheet that the equivalent resistance is $R_{DS-on} = 0.076\Omega$.[22] In the case of the diode, it is obtained from the datasheet that the forward voltage is $V_F = 1.7V$.[23]

3. Commutation region: Switching speeds are equally important parameters for both the MOSFET and the diode. MOSFET switching speed is influenced by its gate-signal, structure, and the circuit topology. On the other hand, the diode switching speed depends on the circuit topology and its structure. Usually MOSFET structure is not considered in the analysis for the reason that it makes the analysis unnecessarily complicated. At this stage, a method will be developed to obtain a rough estimate of the drain current verses time ($I_{DS} vs\ t$). As we know, datasheets only provide graphs for the drain current verses the gate voltage ($V_{GS} vs I_{DS}$) which the manufacturers obtain from various experiments. Therefore it is obvious that we do not have an exact mathematical equation for I_{DS} versus V_{GS}. It is also important to note that one of the major tasks of a power electronics engineer is to construct the desired voltage waveform for the gate ($V_{GS}\ vs\ t$) by accordingly designing gate driver. Again in this case, a designer will have a graph of the waveform without having the exact mathematical equation for $V_{GS}\ vs\ t$. It is apparent that without having these mathematical equations ($I_{DS}\ vs\ V_{GS}$ and $V_{GS}\ vs\ t$) we will not be able to obtain a mathematical expression for the drain current verses time ($I_{DS}\ vs\ t$). To address this issue, below a graphical method will be developed to obtain a rough graph for the drain current verses time ($I_{DS}\ vs\ t$). As it will soon be clear, even though this method is not exact however it may provides a reasonable view of the relationship between the waveforms of drain current and the gate signal, both as

functions of time. The graph in Figure-3.4 consists of four regions which are as follows:

a. Drain current (vertical-axis) versus gate voltage (horizontal-axis). Voltage values start from 4V since pervious values are zero (obtained from the datasheet of APT50M38JFLL)
b. Gate voltage (horizontal-axis) versus time (vertical-axis) (obtained by constructing the gate signal and captured on oscilloscope)
c. Time transformation (graphical mapping)
d. MOSFET drain current (vertical-axis) versus time (horizontal-axis) (result of this graphical method)

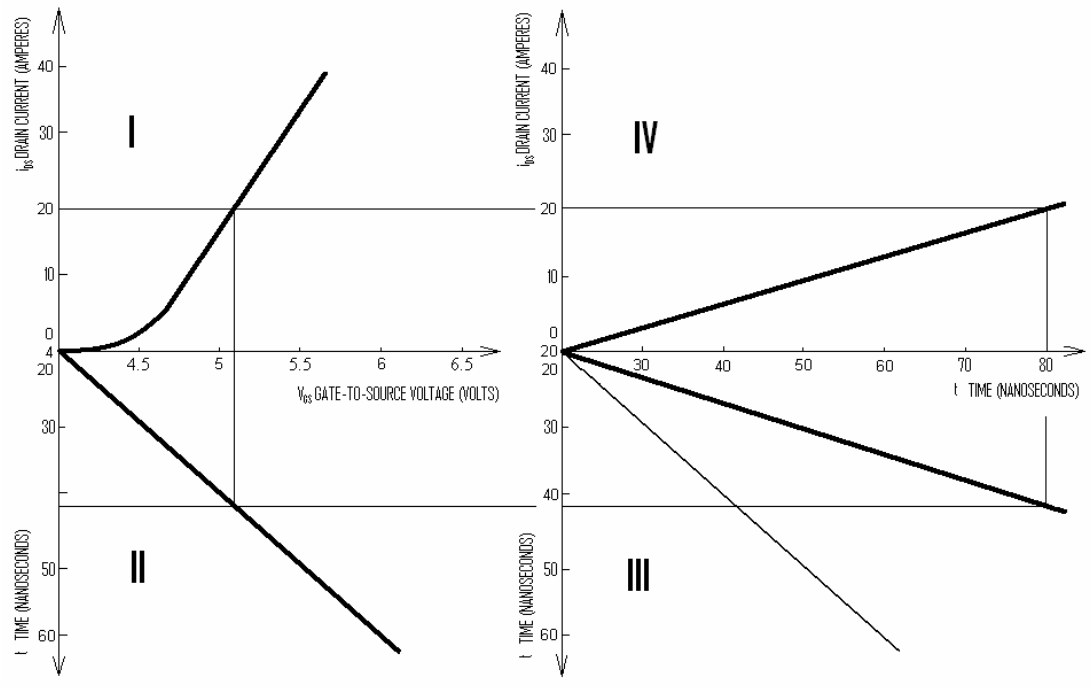

Figure-3.4 Transforming MOSFET static characterizes to dynamic characteristics

The objective of this graphical analysis method is to obtain the waveform of drain current verses time ($I_{DS} vs\ t$) from the waveforms of drain current verses gate voltage ($I_{DS} vs V_{GS}$, obtained from datasheet) and gate voltage verses time ($V_{GS} vs\ t$). Regions I and II show the graphs of $I_{DS} vs V_{GS}$ and $V_{GS} vs\ t$, respectively. From these two graphs we can find out that at a particular instant what gate voltage is applied and furthermore what drain current corresponds to this gate voltage. At first look, it seems that obtaining the drain current verses time ($I_{DS} vs\ t$) is an easy task, since we have the graphs for $I_{DS} vs V_{GS}$ and $V_{GS} vs\ t$. But then it is realized that time delay between the instants when the gate voltage is applied and when the corresponding drain current is achieved need to be considered. This delay makes the analysis somewhat complicated. The delay is due to the fact that a MOSFET can not respond to a certain gate voltage instantaneously. Obtaining the value of this delay is beyond the scope of this analysis and solely depends on the complex device characteristics. On the graph, this delay is represented as the slope of the line in region III; we call this line, the delay line. When the slope of this line is one, this corresponds to zero delay, implying that a particular gate voltage will instantly result in the respective drain current. As the slope increases, bigger delays are represented. In Figure-3.4, the mapping of the drain current with the time axis is shown for the turn-on case. For both cases of MOSFET turn-on and turn-off, the waveforms of $I_{DS}\ vs\ t$ are linearized to obtain the constants, $\frac{di_{ds}}{dt} \approx k$ and $\frac{di_{ds}}{dt} \approx -k'$, as the rising and falling rates respectively. Since the falling and rising rates

of the drain current are comparable, we can assume that their magnitudes are equal. It needs to be emphasized that this method is valid when a voltage source is applied between the drain and the source of the MOSFET. In Figure-3.4, the slope of drain current is found to be 200A/0.8μs. It should be noted that the wire inductance will further decrease the switching speed, so 200A/μs will be used in the calculations instead of 200A/0.8μs.

The following diagram is the revised version obtained from the datasheet of RHRG3060. It illustrates a typical voltage-current waveform for a diode. In most power electronics applications, a diode acts as a capacitor during the turning on and turning off intervals, except in the t_b interval shown in Figure-3.5. It is also important to note that the switching losses only occur in the t_b interval of the reverse recovery.[24, 25] The same signs of the current (-) and the reverse voltage (-) imply power loss. Therefore, designers make an effort to reduce the switching time in order to minimize the switching losses. However, this will have a downside of creating huge overshoot voltages if the rate of reverse recovery (dI_R/dt) is bigger than some threshold. This voltage overshoot can cause failures in the circuit and even destroy the diode.

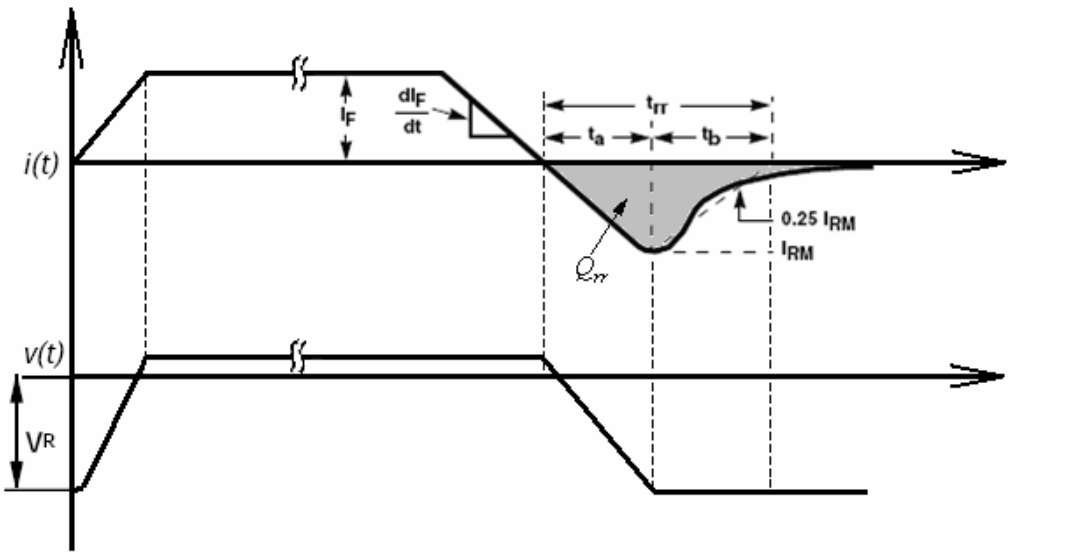

V_F=Forward voltage
I_R=Reverse current
t_{rr}=Reverse recovery time, summation of t_a+t_b
t_a=Time to reach peak reverse current
t_b=Time from peak I_{RM} to projected zero crossing of I_{RM} based on a straight line from peak I_{RM} through 25% of I_{RM}
Q_{RR}=Reverse recovery charge

Figure-3.5 Typical voltage and current waveforms in diode

3.4 Time varying topologies for boost converter

A preliminary discussion of the MOSFET and the diode used in the hard-switching boost converter was presented. At this point, the analysis of hard-switching boost converter will be established. A boost converter, similar to many power electronics circuit is a time variant system. This means that at different time intervals the boost converter can be represented by different topologies, depending on the states

of the semiconductor devices. The following circuits represent the behavior of the topology at particular time intervals. In majority of the literatures, only cutoff and saturation intervals are considered in analyzing the time varying circuits. Here a slightly different approach is taken and commutation intervals are also incorporated in representing the time varying circuits. This is done according to the waveforms of diode and MOSFET voltages and currents as shown in Figure-3.7. As previously discussed, the MOSFET can be modeled as a voltage controlled current source, which occurs in commutation intervals. On the other hand, the Diode can be modeled as a voltage source in this interval.

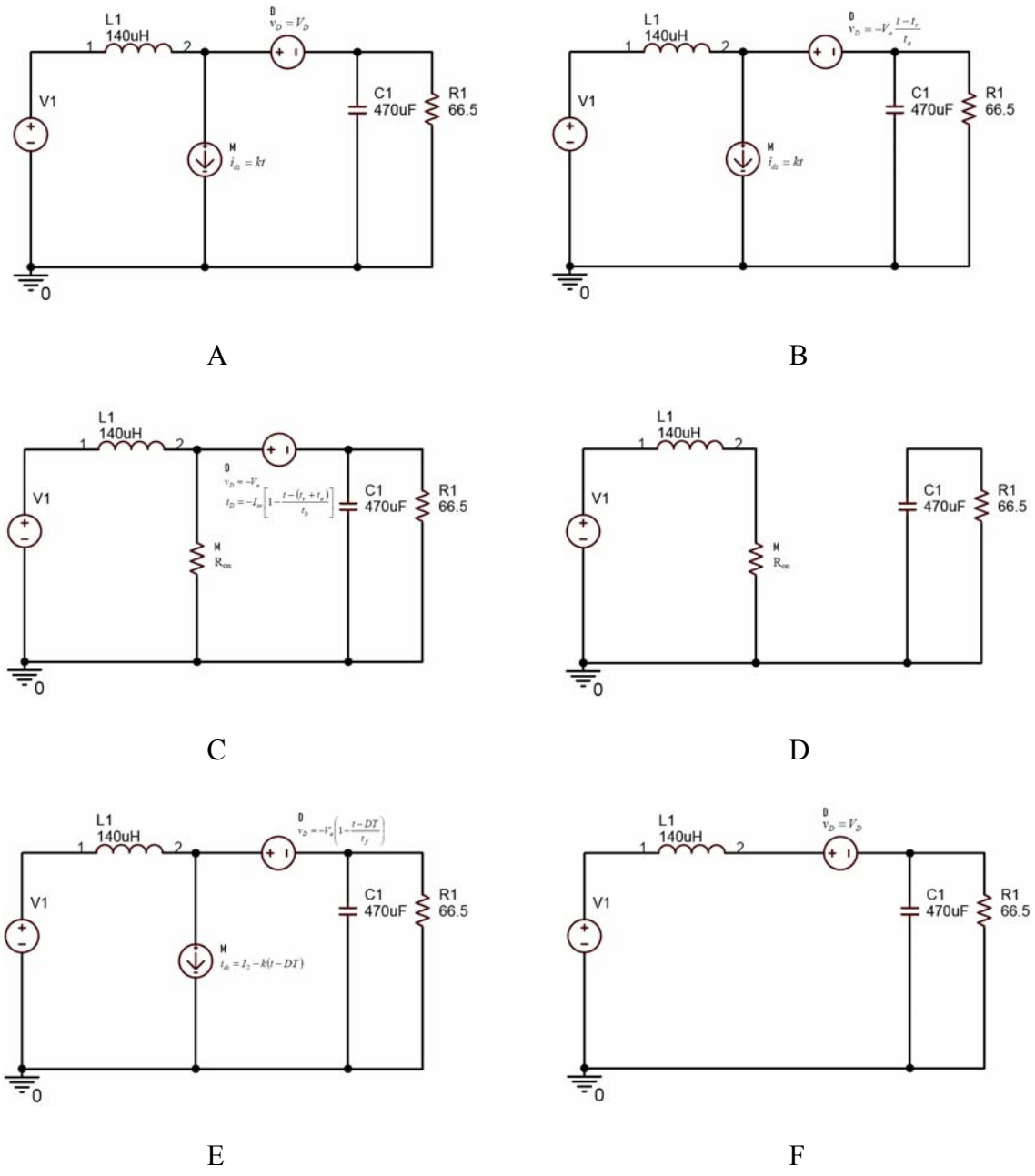

Figure-3.6 Topologies in different intervals (A: internal 1 - turning on MOSFET $0<t<t_r$; B: interval 2 - turning off diode $t_r<t<t_r+t_a$; C: interval 3 - recovering diode $t_r+t_a<t<t_r+t_a+t_b$; D: interval 4 - charging inductor $t_r+t_a+t_b<t<DT$; E: interval 5 - turning off MOSFET $DT<t<DT+t_f$; F: interval 6 - charging Cap $DT<t<DT+t_f$)

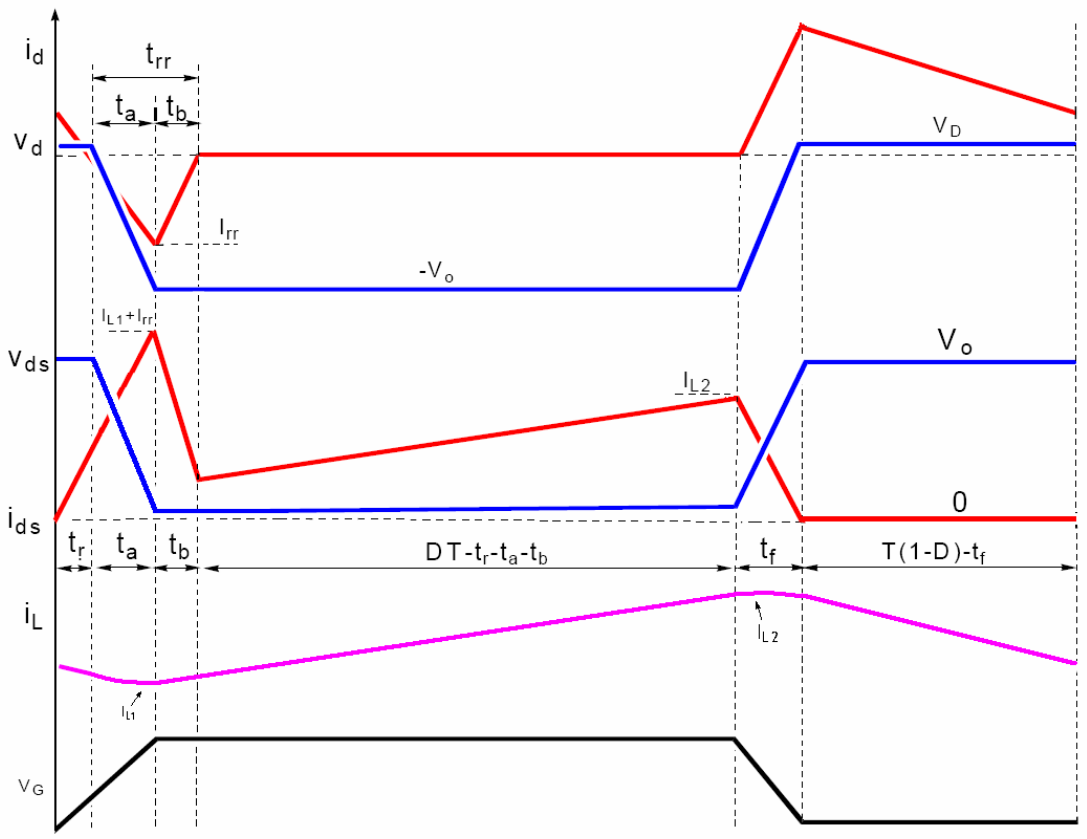

I_1: Minimum inductor current
I_2: Maximum inductor current
D. Duty cycle
T: Period
V_{in}: Input voltage
V_o: Ioutput voltage
R_L: Resistance load
v_{ds}: Drain voltage of MOSFET
i_{ds}: Drain current of MOSFET
t_r: Raise time of MOSFET
t_f: Fall time of MOSFET
Ron: Turn-on resistance of MOSFET
V_F: Forward voltage drop of diode
I_{rr}: Reverse peak current of diode
t_{rr}: Reverse recovery time of diode
Q_{rr}: Reverse recovery charge

Figure-3.7 Diode & MOSFET operating time waveforms

3.5 Mathematical analysis for hard-switching boost converter

For this analysis, the following assumptions are made:

(1) Only operation of the circuit in steady state is considered

(2) The output capacitor is large enough to hold the output voltage as constant

(3) The inductor and capacitor are considered to be ideal

(4) The inductor current is continuous

1. Switching and conduction losses of the MOSFET

a. Turn-on loss: this loss is represented in two parts. In the first part $(0 < t \le t_r)$ the drain voltage remains constant (at the output voltage) while the drain current rises (to reach the inductor current). In the second part $(t_r < t \le t_r + t_a)$, the drain current keeps rising (to $I_{L1} + I_{rr}$) while the drain voltage drops to the saturation voltage. Moreover, the slope of drain current, *k*, depends on the gate signal.

Drain current in the first part: $i_{ds1} = kt$ $(0 < t \le t_r)$

Drain voltage in the first part: $v_{ds1} = V_o$ $(0 < t \le t_r)$

Drain current in the second part: $i_{ds2} = kt$ $(t_r < t \le t_r + t_a)$

Drain voltage in the second part: $v_{ds2} = V_o - \frac{V_o}{t_a}(t - t_r)$ $(t_r < t \le t_r + t_a)$

Average MOSFET turn-on power loss:

$$\overline{P}_{Qturnon} = \frac{1}{T}\left[\int_0^{t_r} V_o kt dt + \int_{t_r}^{t_r+t_a} V_o\left(1 - \frac{t - t_r}{t_a}\right) kt dt\right]$$

$$= \frac{V_o k}{T} \times \frac{3t_r^{\,2} + 3t_r t_a + t_a^{\,2}}{6} \tag{3.1}$$

In order to solve this equation, t_a *and* t_r are obtained as follows:

Drain current of MOSFET: $i_{ds} = kt \qquad (0 < t \le t_r + t_a)$

When $t = t_r$, drain current $i_{ds} = I_{L1} = kt_r$; therefore $t_r = I_{L1}/k$.

When $t = t_r + t_a$, drain current $i_{ds} = I_{L1} + I_{rr} = k(t_r + t_a)$; therefore $t_a = I_{rr}/k$.

Substituting t_r and t_a in Equation-3.1:

$$\overline{P}_{Qturnon} = \frac{V_o\left(3I_{L1}^{\,2} + 3I_{L1}I_{rr} + I_{rr}^{\,2}\right)}{6kT} \tag{3.2}$$

Approximation of turn-on power stress:

$$\overline{P}_{Qon-stress} = T\overline{P}_{Qturnon}/(t_r + t_a) = \frac{V_o\left(3I_{L1}^{\,2} + 3I_{L1}I_{rr} + I_{rr}^{\,2}\right)}{6\left(I_{L1} + I_{rr}\right)} \approx \frac{V_o\left(3I_{L1} + I_{rr}\right)}{6}$$

b. Turn-off loss – during the interval t_f, the drain current drops to the leakage current while the drain voltage increases to the output voltage. Moreover, we can assume that the slope of the drain current is (–*k*).

Drain current: $i_{ds} = I_{L2} - kt \qquad (0 < t < t_f)$

Drain voltage: $v_{ds} = \frac{V_o}{t_f} t \qquad (0 < t < t_f)$

Average MOSFET turn-off power loss:

$$\overline{P}_{Qturnoff} = \frac{1}{T}\int_0^{t_f}\left[\frac{V_o}{t_f}\left(I_{L2}t - kt^2\right)\right]dt$$

$$= \frac{V_o}{T}\left(\frac{1}{2} I_{L2} t_f - \frac{1}{3} k {t_f}^2\right) \tag{3.3}$$

When $t = t_f$, drain current $i_{ds} = I_{L2} - kt_f = 0$; therefore $t_f = I_{L2}/k$.

Substituting t_f in Equation-3.3 yields:

$$\overline{P}_{Qturnoff} = \frac{V_o {I_{L2}}^2}{6kT} \tag{3.4}$$

Approximate turn-off power stress:

$$\overline{P}_{Qoff-stress} = T\overline{P}_{Qturnoff} / t_f = \frac{V_o I_{L2}}{6}$$

c. Conduction loss –conduction loss depends on the drain current and MOSFET structure. This loss has to be calculated in order to determine the efficiency of the system. Moreover, knowledge of this loss will enable designer to estimate the junction temperature and design appropriate heat sink.

Drain current: $i_{ds} = I_{L1} + \frac{I_{L2} - I_{L1}}{DT - t_r - t_a} t \qquad (0 < t < DT - t_r - t_a)$

Average turning-off power loss of MOSFET:

$$\overline{P}_{Qon} = \frac{1}{T}\int_0^{DT-t_r-t_a} R_{on}\left(I_{L1} + \frac{I_{L2} - I_{L1}}{DT - t_r - t_a} t\right)^2 dt$$

$$= \frac{DT - t_r - t_a}{3T}\left({I_{L2}}^2 + I_{L2} I_{L1} + {I_{L1}}^2\right) R_{on} \tag{3.5}$$

Substituting $t_r = I_{L1}/k$ and $t_a = I_{rr}/k$ into the above equation:

$$\overline{P}_{Qon} = \frac{DTk - I_{L1} - I_{rr}}{3Tk}\left({I_{L2}}^2 + I_{L2} I_{L1} + {I_{L1}}^2\right) R_{on} \tag{3.6}$$

2. Switching and conduction losses of the diode

a. Switching loss – as mentioned before, this loss only occurs during the t_b interval.

Reverse recovery current: $i_{rr} = -\frac{I_{rr}}{t_b} t \qquad (0 < t < t_b)$

Reverse voltage: $v_{D-reverse} = -V_o \qquad (0 < t < t_b)$

Average switching power loss of the diode:

$$\overline{P}_{Dswitching} = \frac{1}{T}\int_0^{t_b} -V_o\left(-\frac{I_{rr}}{t_b} t\right) dt$$

$$= \frac{V_o I_{rr} t_b}{2T} \tag{3.7}$$

Reverse recovery charge: $Q_{rr} = \frac{I_{rr}\left(t_a + t_b\right)}{2}$

$$t_b = \frac{2Q_{rr}}{I_{rr}} - t_a$$

$$t_a = \frac{I_{rr}}{k}$$

Therefore:

$$t_b = \frac{2Q_{rr}}{I_{rr}} - \frac{I_{rr}}{k}$$

Substituting t_b into Equation-3.7:

$$\overline{P}_{Dswitching} = \frac{V_o}{T}\left(Q_{rr} - \frac{{I_{rr}}^2}{2k}\right) \tag{3.8}$$

b. Conduction loss – this loss is caused by the forward current and constant forward voltage.

Forward current: $i_D = I_{L2} + \frac{I_{L1} - I_{L2}}{T - DT - t_f} t$

Forward voltage: $v_D = V_D$

Average conduction power loss of diode:

$$\overline{P}_{Don} = \frac{1}{T}\int_0^{T-DT-t_f} V_D \left(I_{L2} + \frac{I_{L1} - I_{L2}}{T - DT - t_f} t \right) dt$$

$$= \frac{V_D (I_{L1} + I_{L2})(T - DT - t_f)}{2T} \qquad (3.9)$$

Substituting $t_f = I_{L2} / k$ into Equation-3.9:

$$\overline{P}_{Don} = \frac{V_D (I_{L1} + I_{L2})(T - DT - I_{L2} / k)}{2T} \qquad (3.10)$$

3. Average inductor current: Now the average inductor current is calculating by taking the time average of inductor current in each of the intervals indicated below.

a. Turning-on process of the MOSFET – this process occurs in three intervals (t_r, t_a, t_b), but interval t_r can be added to the interval that the diode is on ($T(1-D)-t_f$), and interval t_b can be added to the interval that the MOSFET is on ($DT-t_r-t_a-t_b$) in order to simplify the calculation. Therefore turning-on process of the MOSFET only has the interval t_a and all the expressions in Figure-3.6 need to be shifted by time, t_r.

Refer to the Figure-3.6 Interval-2 topology $(0 < t < t_a)$.

$$V_{in} - \left[-V_o \frac{(t - t_r) + t_r}{t_a} \right] - V_o = L \frac{di_L}{dt}$$

$$V_{in} + V_o \frac{t}{t_a} - V_o = L \frac{di_L}{dt}$$

$$i_L(t) = \frac{V_o t^2}{2Lt_a} + \frac{(V_{in} - V_o)t}{L} + i_L(0) \qquad (0 < t < t_a)$$

$$i_L(t_a) = \frac{(2V_{in} - V_o)t_a}{2L} + i_L(0)$$

Contribution of the average inductor current due to the interval $(0 < t < t_a)$:

$$\overline{i_{L1}} = \frac{1}{T}\int_0^{t_a} i_L(t)dt$$

$$= \frac{1}{T}\left[\frac{(3V_{in} - 2V_o)t_a^{\,2}}{6L} + t_a i_L(0)\right] \qquad (3.11)$$

b. On-state of the MOSFET (including t_b interval): in the interval t_b, the drain current of the MOSFET is the sum of reverse recovery current of the diode and the inductor current. The voltage drop which is caused by the reverse recovery current also influences the inductor current, but it is disregarded here because of the small values of t_b and R_{on}.

Refer to Figure-3.6- Interval-4 topology $(t_a < t < DT - t_r)$:

$$V_{in} = L \frac{di_L}{dt} + i_L R_{on}$$

$$i_L(t) = \frac{V_{in}}{R_{on}} - \exp\left\{-\frac{t - t_a}{L / R_{on}}\right\}\left[\frac{V_{in}}{R_{on}} - i_L(t_a)\right] \qquad (t_a < t < DT - t_r)$$

$$\approx \frac{V_{in}}{L}(t - t_a) + i_L(t_a)\left[1 - \frac{R_{on}(t - t_a)}{L}\right] \qquad \left(\because \exp\left\{-\frac{t - t_a}{L / R_{on}}\right\} \approx 1 - \frac{t - t_a}{L / R_{on}}\right)$$

$$i_L(DT-t_r)=\frac{V_{in}}{L}(DT-t_r-t_a)+i_L(t_a)\left[1-\frac{R_{on}(DT-t_r-t_a)}{L}\right]$$

Contribution of the average inductor current due to the interval $(t_a < t < DT-t_r)$:

$$\overline{i_{L2}}=\frac{1}{T}\int_{t_a}^{DT-t_r} i_L(t)dt$$

$$=\frac{(DT-t_r-t_a)^2[V_{in}-R_{on}i_L(t_a)]+2L(DT-t_r-t_a)i_L(t_a)}{2TL} \qquad (3.12)$$

c. Turning-off process of MOSFET

Refer to Figure-3.6-Interval-5 topology $(DT-t_r < t < DT-t_r+t_f)$:

$$V_{in}-\left\{-V_o\left[1-\frac{t-(DT-t_r)}{t_f}\right]+V_o\right\}=L\frac{di_L}{dt} \qquad (DT-t_r < t < DT-t_r+t_f)$$

$$V_{in}-V_o\frac{t-(DT-t_r)}{t_f}=L\frac{di_L}{dt}$$

$$i_L(t)=-\frac{V_o[t-(DT-t_r)]^2}{2Lt_f}+\frac{[t-(DT-t_r)]V_{in}}{L}+i_L(DT-t_r)$$

$$i_L(DT-t_r+t_f)=\frac{t_f(2V_{in}-V_o)}{2L}+i_L(DT-t_r)$$

Contribution of the average inductor current due to the interval

$(DT-t_r < t < DT-t_r+t_f)$:

$$\overline{i_{L3}}=\frac{1}{T}\int_{DT-t_r}^{DT-t_r+t_f} i_L(t)dt$$

$$=\frac{1}{T}\left[\frac{(3V_{in}-V_o)t_f^{\,2}}{6L}+i_L(DT-t_r)t_f\right] \qquad (3.13)$$

d. Off-state of the MOSFET (including the t_a interval):

Refer to Figure-3.6-Interval-6 topology $\left(DT - t_r + t_f < t < T\right)$:

$$\frac{L\left\{i_L(t) - i_L\left(DT - t_r + t_f\right)\right\}}{t - \left(DT - t_r + t_f\right)} = V_{in} - V_D - V_o \qquad \left(DT - t_r + t_f < t < T\right)$$

$$i_L(t) = \frac{\left(V_{in} - V_D - V_o\right)\left[t - \left(DT - t_r + t_f\right)\right]}{L} + i_L\left(DT - t_r + t_f\right)$$

$$i_L(T) = \frac{\left(V_{in} - V_D - V_o\right)\left[T - \left(DT - t_r + t_f\right)\right]}{L} + i_L\left(DT - t_r + t_f\right)$$

Contribution of the average inductor current due to the interval

$\left(DT - t_r + t_f < t < T\right)$:

$$\overline{i_{L4}} = \frac{1}{T}\int_{DT - t_r + t_f}^{T} i_L(t)dt$$

$$= \frac{1}{T}\left\{\frac{\left(V_{in} - V_D - V_o\right)\left[T - \left(DT - t_r + t_f\right)\right]^2}{2L} + i_L\left(DT - t_r + t_f\right)\left(T - DT + t_r - t_f\right)\right\} \qquad (3.14)$$

According to the above expressions for the inductor current, two approximations need to be made:

1. the minimum inductor current, $I_{L1} \approx i_L(0)$
2. the maximum inductor current, $I_{L2} \approx i_L\left(DT - t_r\right)$

Finally total average inductor current can be obtained as follows:

$$\overline{i_L} = \overline{i_{L1}} + \overline{i_{L2}} + \overline{i_{L3}} + \overline{i_{L4}} \qquad (3.15)$$

The inductor continuous current equation:

$$i_L(0) = i_L(T) \neq 0 \qquad (3.16)$$

Power Balance equation:

$$V_{in}\overline{i_L} = \frac{V_o^{\,2}}{R_L} + \overline{P}_{Qturnon} + \overline{P}_{Qturnoff} + \overline{P}_{Qon} + \overline{P}_{Dswitching} + \overline{P}_{Don}\,. \qquad (3.17)$$

3.6 A method to calculate duty cycle and minimum and maximum inductor currents (D, I_{L1}, I_{L2})

The aim of these calculations is to obtain the power losses in the semiconductor devices (MOSFET and diode). Numerical method is used in MATLAB for this purpose in order to take advantage of the computer's utility. First guess value is used for I_{L1} in Equation-3.16 to obtain the duty cycle. At the same time I_{L2} is obtained. At this point we have all the trial values for D, I_{L1}, I_{L2} and based on this the losses are calculated according to the respective equations states above. Next these power loss values are continuously tested in the power balance Equation-3.17 and if this equation is satisfied then the solution is reached.

3.7 The analytical result and hardware-test result

For these calculations the following parameters were used:

$$\begin{cases} L = 140uH \\ V_{in} = 60V \\ V_o = 200V \\ R_L = 66.5\Omega \end{cases} \tag{3.18}$$

$$\begin{cases} k = 200A/us \\ I_{rr} = 2 \times 4.6A \\ Q_{rr} = 100nc \\ R_{on} = 76m\Omega \\ V_D = 1.7V \end{cases} \tag{3.19}$$

$$\eta = \frac{\frac{V_o^{\,2}}{R_L}}{V_{in} I_{in}} \tag{3.20}$$

Figure-3.8 shows the total loss in each of the semiconductor devices (MOSFET and diode), obtained from the above analysis. The results from the hardware test are summarized in Table-3.1. Equation-3.20 is used to calculate the efficiency of the system. Since in this equation, V_o, V_{in}, and R_L are all constants, I_{in} is the only variable that influences the efficiency. Figure-3.9 shows the efficiency of the converter, which is obtained from the analytic method and hardware test.

Table-3.1 Input current versus operating frequency (hardware test)

Frequency (kHz)	25.0	51.3	76.0	99.0	125
Input Current (A)	10.14	10.16	10.24	10.29	10.45
Efficiency	0.989	0.987	0.979	0.974	0.959

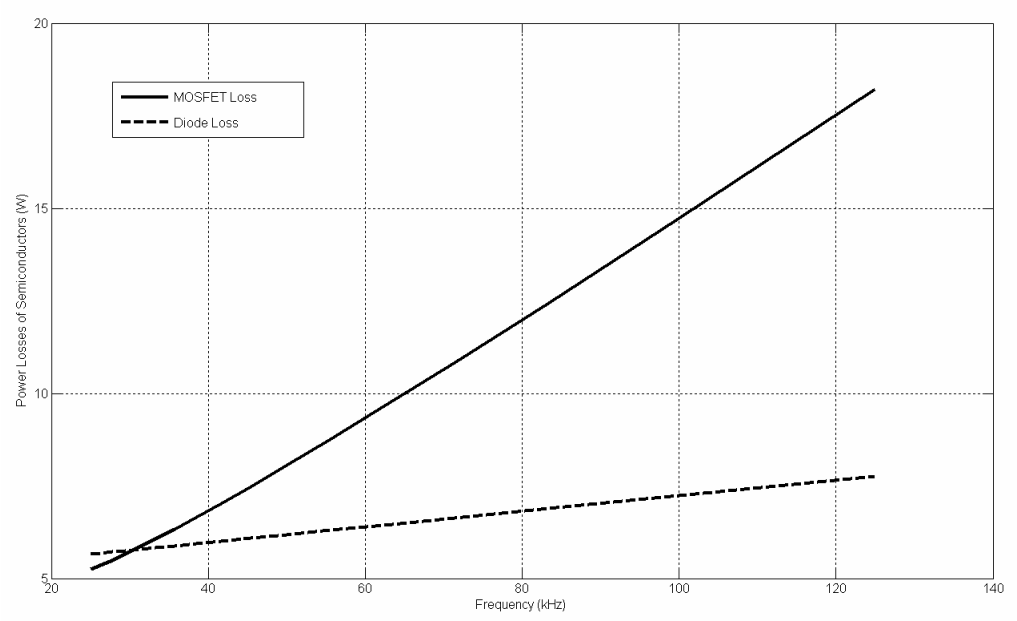

Figure-3.8 MOSFET loss and diode loss versus frequency

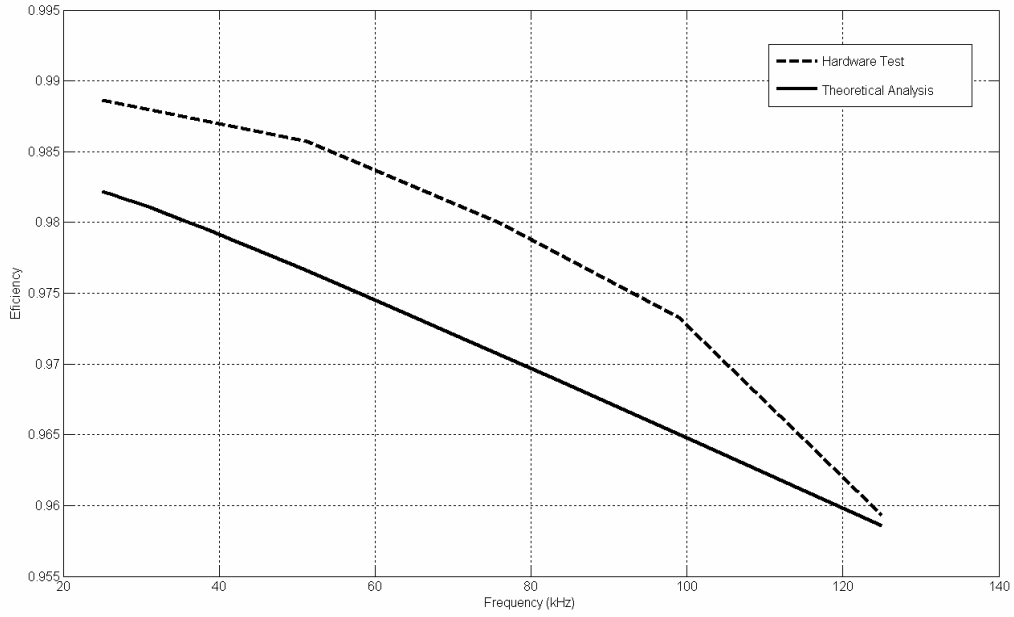

Figure-3.9 Theoretical analysis and hardware test versus frequency

As shown in Figure-3.9, the graph for the calculated efficiency is a linear function of the frequency. This is because nonlinear effects of frequency on the power loss are not considered in our analytic method. These effects show up on the graph obtained from the hardware tests. In calculating the losses, an effort was made to consider the worse case scenario. Therefore, the actual losses for the system were expected to be below the calculated ones. Based on the information represented on the above graphs, a designer is able to estimate losses for each of the semiconductor devices for the purpose of determining the efficiency of the converter. Also this information can be used in selecting a heat sink with an appropriate thermal resistance so as to avoid crossing the maximum allowed junction temperature.

It is seen that, the above analytical methods provide a systematic way to obtain different power losses by the knowledge of maximum and minimum inductor currents and also the duty cycle (I_{L1}, I_{L2} and D). It is also important to note that setting up all the necessary equations for this analysis is somewhat cumbersome and complicated. Because of this a simpler method will be introduced. The steps to apply this method are as follows. First all the losses are transferred to the output side. This will allow the consideration of boost converter as an ideal model. Next numerical method is used in MATLAB for this purpose in order to take advantage of the computer's utility. With the first guess value as the total losses, an ideal model is used to calculate D, I_{L1}, I_{L2}. At this point we have all the trial values for D, I_{L1}, I_{L2} and based on this the losses are calculated according to the respective power loss equations states above. Next these

power loss values are continuously tested in the power balance Equation-3.17 and if this equation is satisfied then the solution is reached.

CHAPTER 4

SOFT-SWITCHING BOOST CONVERTER

4.1 Introduction of soft switching technology

It was shown in Chapter-3 that semiconductor devices consume considerable power losses at high frequencies. Moreover, power stress dramatically reduces semiconductor lifetime. On the other hand, converters at high switching frequencies have the advantage of requiring smaller components which also makes them cost efficient. With advances in semiconductor technology, hard switching power electronics circuits have added efficiency and reliability; however, for the most part the problem of high electrical noise is still present. Therefore, we need to reduce high frequency harmonics that is caused by the sharp edges of voltage and current waveforms in semiconductor switches. We accomplish this by incorporating inertia components (inductors and capacitors) that effectively reduce di/dt and dv/dt. At the same time, it is desirable to reduce the switching losses which for the most part are caused by the overlapping of high voltages and currents in a switch. Therefore, we will be able to decrease the losses by either smoothing out currents and/or voltages in the switches, and by creating a delay between them. This is the idea behind using snubber circuits in order to achieve reduced losses and noise. The snubber circuits are classified as passive and active. Passive snubber circuits use passive components such as inductors and capacitors. On the other hand, the active snubber circuits incorporate

controllable semiconductor switches. Snubbers are primarily required in power electronics applications to keep the devices within their safe operating areas.[26,27] Resistors were used in the old fashion snubber circuits, which is not practical at high frequency. Therefore resonant snubber circuits were later developed, which do not involve resistive components. Resonant snubbers are almost completely lossless, but they tend to oscillate.[28] In the following design, this drawback will be considered and a method is utilized in order to avoid this.

4.2 Soft switching boost converter design

As mentioned before, boost converter is suited for fuel cell applications since it draws continuous current. In other words, at high power applications, the continuous-conduction-mode boost converter is the preferred topology with continuous input-current. As a result, in recent years, significant efforts have been invested on improving the performance of high-power boost converters.[29,30,31] The majority of these development efforts have been focused on reducing the adverse effects of the reverse recovery characteristic of the boost diode. The reveres recovery current reduces efficiency and creates EMC concerns.[32] As illustrated in Figure-3.7, the high rate at which current drops to zero results in a huge reverse recovery current. As indicated in Equation-3.2, high reverse recovery current implies increased switching losses. In the design of a converter, snubber circuits are used in order to alleviate the reverse recovery current. Generally, passive lossless snubbers are as effective as their active counterparts in reducing the reverse-recovery-current. However the passive subbers do not offer

ZVS to eliminate the switching losses and hence generate significant current or voltage stress for the devices.[33] This increased current-and-voltage stresses demand high rated and usually more expensive components. Moreover, high circulating currents cause more conduction losses in this type of circuit. However, active snubbers can be utilized in order to realize ZCS (zero current switching) and ZVS (zero voltage switching) in switches and therefore reduce losses. In applications such as fuel cells that provide low voltages and high currents, switching losses become significant, as indicated by Equation-3.2. As seen in this equation, power loss is proportional to the square of the input current to the converter. In other words, for the same value of input power, the losses can be significantly higher for a converter that has a bigger input current. The use of ZVS techniques significantly improves the efficiency of the high power boost converter by reducing the turn-on losses. As shown in Figure-4.1, ZVS is realized by using an auxiliary MOSFET, together with a resonant inductor, to transfer the energy stored in the main MOSFET to the output capacitor; otherwise this energy would turn into switching losses. In other words, turn-on switching losses of the boost MOSFET are turned into useful output power. When the auxiliary switch is turned on, the drain voltage of the main MOSFET can drop to zero to realize ZVS. If a capacitor is paralleled with main MOSFET M_1, its drain voltage rate can be reduced in turn-off, so that the turn-off loss of M_1 can also be reduced. The topology is shown in Figure-4.2. When main switch M_1 is turned on, L_2 and the parasitic capacitor of M_2 form an oscillating loop. This oscillating current can cause additional losses if not taken care of. For this purpose we add a diode, D_3, to block the circulating current. Also saturable

reactor is added to damp the oscillation, but this element is not considered in the analysis for the sake of simplicity. Since the rms current value is small in the resonant inductor, small auxiliary MOSFET (M_2) and diode (D_3) are employed.[34, 35, 36]

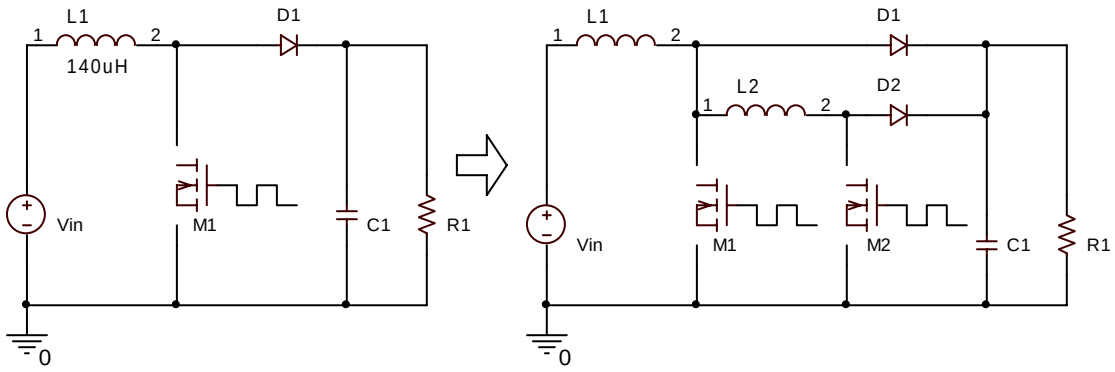

Figure-4.1 Boosting turn-on loss to the output

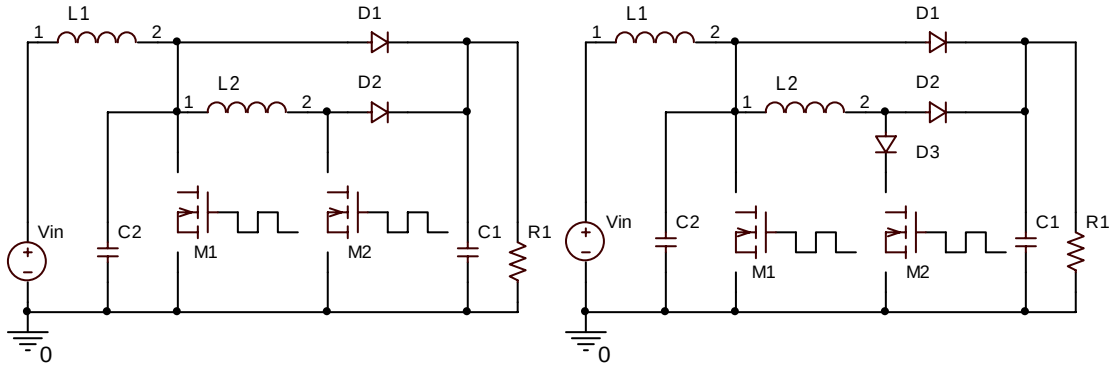

A B

Figure-4.2 A. Reducing turn-off dv/dt ; B. reduction of circulating current

4.3 Analysis of soft switching boost converter at different intervals

In Chapter-3, a method was introduced that incorporates the ideal model of the converter along with the power loss equations to simplify the analysis. In this method the losses are transferred to the output side. This allows us to calculate power losses based on currents and voltages from the ideal model. In this section, ideal models will be used to analyze the soft switching boost converter. Figure-4.3 shows voltage and current waveforms for all the semiconductor devices (M_1, M_2, D_1, D_2) and will be referred to often in the consideration of power losses in different operating intervals. Before starting the methodical analysis, some assumptions need to be made:

1. Only the operation of the circuit in steady state is considered for power-loss analysis.
2. The output capacitor is large enough to hold the output voltage sufficiently constant for the power-loss analysis.
3. The main inductor current is continuous.
4. Oscillations in the auxiliary MOSFET are avoided in the analysis. As mentioned before, this effect was reduced to an acceptable amount by utilizing a damping diode and saturable reactor. These oscillations are indicated in Figure-4.3 with hashed lines.
5. When the main MOSFET drain voltage drops to zero, voltage detector (logic output circuit) sends a signal to the controller IC and action is taken to turn on the main MOSFET. The resulted delay time is neglected since it does not have any significant ramification.

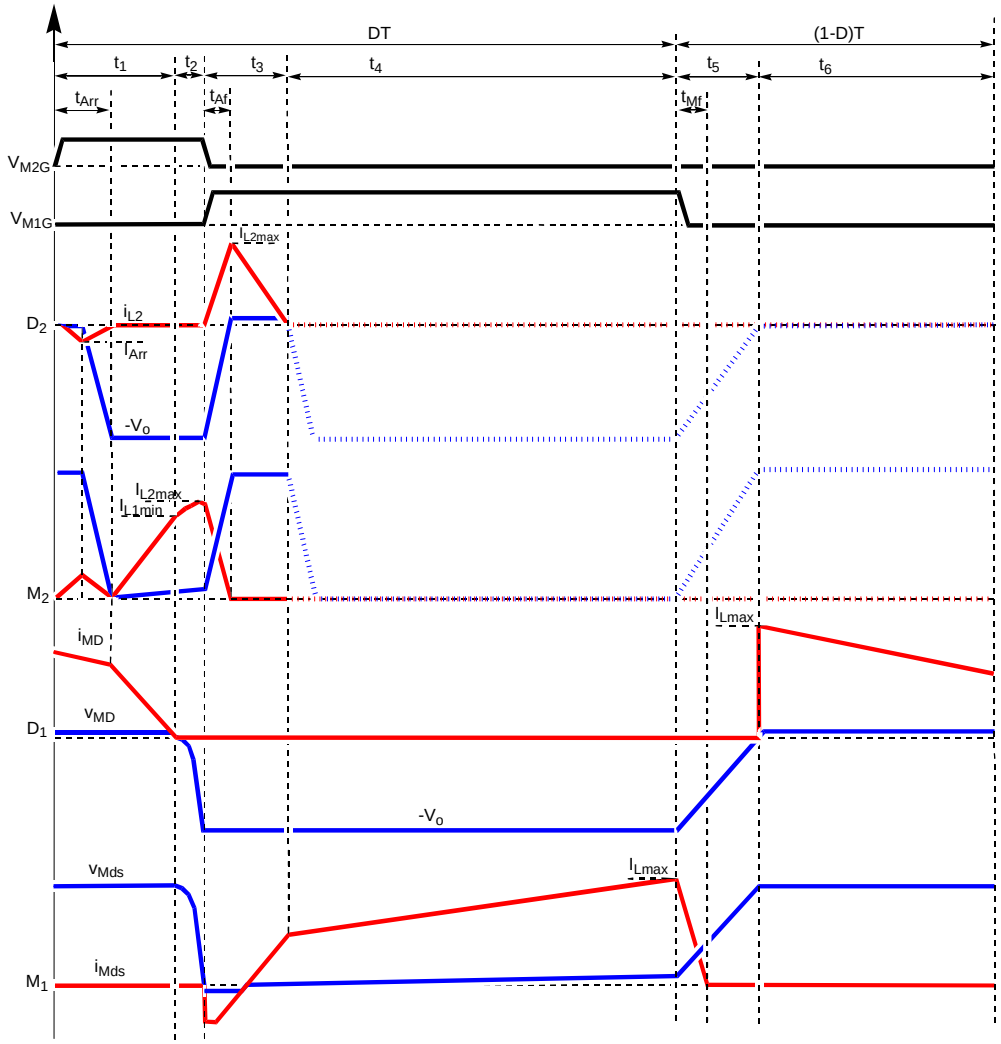

Figure-4.3 Voltage and current waveforms for the switches (M1, M2, D1, D2) that indicate the operating intervals for the ideal topologies

The above figures signify waveforms for the semiconductor devices during one period, *T*. Variable definitions for the analysis are given:

C_1, C_2: output and resonant capacitors

D: duty cycle

I_{L1min}, I_{L1max}: main inductor minimum and maximum currents

I_{Amax}: resonant inductor peak current

I_{Arr}: auxiliary diode reverse recovery peak current

k: current rising rate

L_1, L_2: main inductor and resonant inductor

R_1: resistance load

R_{Aon}, R_{Mon}: auxiliary and main MOSFET turn-on resistances

t_{Arr}: auxiliary diode reverse recovery time

t_{Mf}, t_{Af}: main and auxiliary MOSFET fall times

V_{in}, V_o: input and output voltages

V_{D1}, V_{D2}: main and auxiliary diode forward voltage drops

Analysis of soft-switching boost converter is as follows:

a. The ideal topology for the first interval $(0 < t < t_1)$ is shown in Figure-4.4. At the start of this interval, auxiliary MOSFET M_2 is turned on while the main diode D_1 is on and main MOSFET M_1 is off. Auxiliary diode D2 undergoes reverse recovery because of previous zero-voltage across it. At this time D_2 becomes reversed biased and turns off. Also since output voltage is being applied to L_2, current starts to build up in this inductor. As it can be inferred from the figure, current through D_1 gradually swaps over to L_2. The current in D_1 reaches zero (soft turn-off) at the end of this interval.

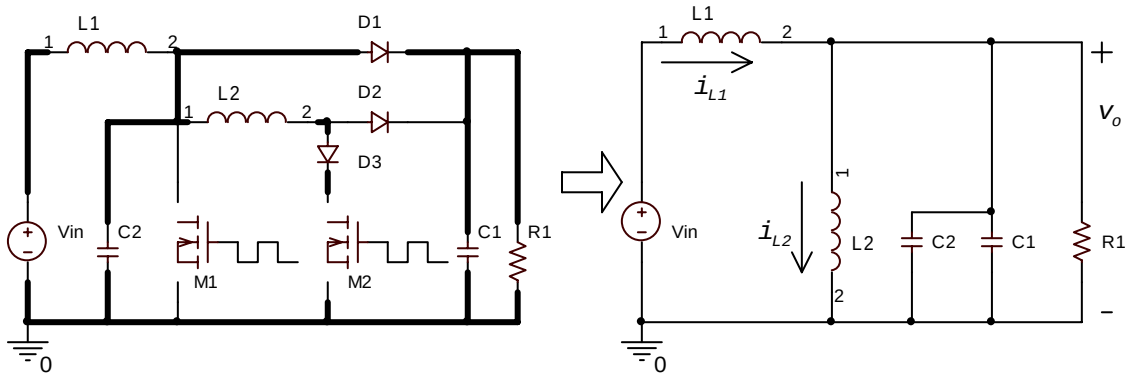

Figure-4.4 Ideal equivalent circuit when M_2 and D_1 are on

All voltages and currents are defined according to the sign convention. KVL & KCL are expressed as:

$$-V_{in} + L_1 \frac{di_{L1}}{dt} + V_{C1} = 0 \tag{4.1}$$

$$-L_2 \frac{di_{L2}}{dt} + V_{C1} = 0 \tag{4.2}$$

$$i_{L1} - i_{L2} - (C_1 + C_2)\frac{dv_{C1}}{dt} - \frac{v_{C1}}{R_1} = 0 \tag{4.3}$$

$$i_{L1} - i_{L2} - (C_1 + C_2)\frac{dv_{C2}}{dt} - \frac{v_{C2}}{R_1} = 0 \tag{4.4}$$

In the matrix form for the above equations:

$$\begin{bmatrix} \frac{di_{L1}}{dt} \\ \frac{di_{L2}}{dt} \\ \frac{dv_{C1}}{dt} \\ \frac{dv_{C2}}{dt} \end{bmatrix} = \begin{bmatrix} 0 & 0 & \frac{-1}{L_1} & 0 \\ 0 & 0 & \frac{1}{L_2} & 0 \\ \frac{1}{C_1 + C_2} & \frac{-1}{C_1 + C_2} & \frac{-1}{R_1(C_1 + C_2)} & 0 \\ \frac{1}{C_1 + C_2} & \frac{-1}{C_1 + C_2} & 0 & \frac{-1}{R_1(C_1 + C_2)} \end{bmatrix} \begin{bmatrix} i_{L1} \\ i_{L2} \\ v_{C1} \\ v_{C2} \end{bmatrix} + \begin{bmatrix} \frac{V_{in}}{L_1} \\ 0 \\ 0 \\ 0 \end{bmatrix} \tag{4.5}$$

For the power analysis, only steady state is considered. In other words, V_o is equal to V_{C1} and is considered constant. It is necessary to calculate both inductor-current i_{L1} and i_{L2} to obtain power losses. From Equation-4.1 and 4.2 inductor currents are obtained as shown:

$$\begin{cases} i_{L1} = \dfrac{V_{in} - V_o}{L_1} t + i_{L1}\big|_0 \\ i_{L2} = \dfrac{V_o}{L_2} t \end{cases}, \text{ where } \begin{cases} i_{L1}\big|_0 = i_{L1}\big|_T \\ i_{L2}\big|_0 = 0 \end{cases} \text{ and } (0 < t < t_1) \tag{4.6}$$

$$\because \frac{V_{in} - V_o}{L_1} t_1 + i_{L1}\big|_0 = \frac{V_o}{L_2} t_1$$

$$\therefore t_1 = \frac{L_1 L_2 i_{L1}\big|_0}{(L_1 + L_2) V_o - L_2 V_{in}} \approx \frac{L_2 i_{L1}\big|_0}{V_o} \ (\text{Since } L_2 << L_1) \tag{4.7}$$

$$i_{L1}\big|_{t1} = \frac{L_2 V_{in} + (L_1 - L_2) V_o}{L_1 V_o} i_{L1}\big|_0 \tag{4.8}$$

The power losses in this interval include turn-on loss and conduction loss in auxiliary MOSFET M_2, switching loss in auxiliary diode D_2, conduction loss in main diode D_1, and conduction loss in damping diode D_3. However, entire turn-on loss ($\overline{P}_{M2turn-on}$) in M_2 and switching loss $\left(\overline{P}_{D2switching}\right)$ in D_2 only occur in this interval. According to Equation-3.2, 3.7 respectively, the losses can be obtained as shown:

$$\overline{P}_{M2turn-on} = \frac{V_o {I_{Arr}}^2}{6kT} \tag{4.9}$$

$$\overline{P}_{D2switching} \approx \frac{V_o I_{Arr} t_{Arr}}{4T}, \text{ where } t_{Ab} \approx t_{Arr} \Big/ 2 \tag{4.10}$$

Since it is easier to express conduction loss of a device as a single equation (not considered separately at different intervals) all the involved conduction losses will be considered in the following steps.

b. The ideal topology for the interval $(t_1 < t < t_1 + t_2)$ is shown in Figure-4.5. At this interval, auxiliary MOSFET M_2 is still on; then the drain voltage of main MOSFET M_1 starts to drop to zero since resonant inductor L_2 discharges resonant capacitor C_2 which is paralleled with M_1. Drain voltage of M_1 will drop to zero by the end of this interval; thereby ZVS will be achieved for M_1.

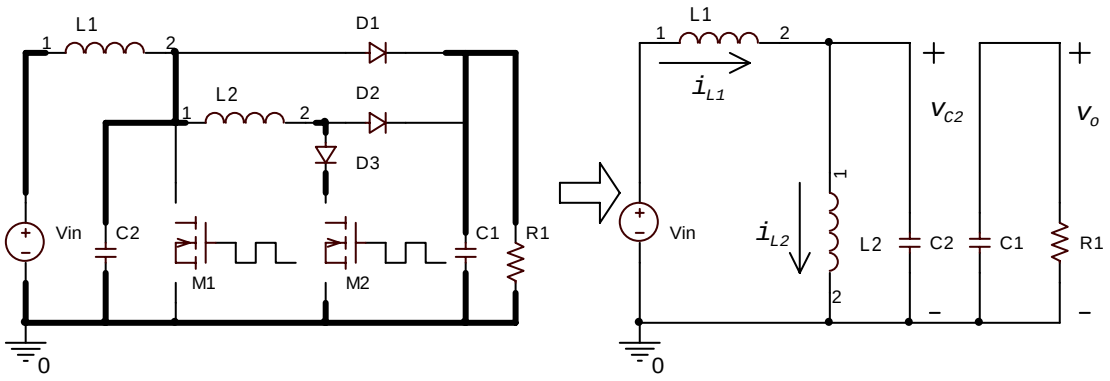

Figure-4.5 Ideal equivalent topology when M_2 is on

All voltages and currents are defined according to the sign convention. KVL & KCL are expressed as:

$$-V_{in} + L_1 \frac{di_{L1}}{dt} + V_{C2} = 0 \qquad (4.11)$$

$$-L_2 \frac{di_{L2}}{dt} + V_{C2} = 0 \qquad (4.12)$$

$$-C_1 \frac{dv_{C1}}{dt} - \frac{v_{C1}}{R_1} = 0 \qquad (4.13)$$

$$i_{L1} - i_{L2} - C_2 \frac{dv_{C2}}{dt} = 0 \tag{4.14}$$

In the matrix form for the above equations:

$$\begin{bmatrix} \frac{di_{L1}}{dt} \\ \frac{di_{L2}}{dt} \\ \frac{dv_{C1}}{dt} \\ \frac{dv_{C2}}{dt} \end{bmatrix} = \begin{bmatrix} 0 & 0 & 0 & \frac{-1}{L_1} \\ 0 & 0 & 0 & \frac{1}{L_2} \\ 0 & 0 & \frac{-1}{R_1 C_1} & 0 \\ \frac{1}{C_2} & \frac{-1}{C_2} & 0 & 0 \end{bmatrix} \begin{bmatrix} i_{L1} \\ i_{L2} \\ v_{C1} \\ v_{C2} \end{bmatrix} + \begin{bmatrix} \frac{V_{in}}{L_1} \\ 0 \\ 0 \\ 0 \end{bmatrix} \tag{4.15}$$

In practice, C_2 is selected to be around 500pF and L_1 more than 10 times of L_2; therefore, L_1 can be considered as a constant current source when analyzing the resonant-inductor current. That is, the energy stored in resonant capacitor C_2 will be transferred to resonant inductor L_2. The maximum current in L_2 is given by:

$$I_{A\max} = \sqrt{\left(i_{L2}\big|_{t1}\right)^2 + \frac{C_2}{L_2} V_o^{\,2}} \tag{4.16}$$

Final value of main inductor current is given by:

$$i_{L1}\big|_{t1+t2} = i_{L1}\big|_{t1} \tag{4.17}$$

Since C_2 and L_2 form a resonant circuit, interval t_2 is ¼ of the resonant period (voltage across C_2 drops to zero at the end of this interval):

$$t_2 = \frac{\pi\sqrt{L_2 C_2}}{2} \tag{4.18}$$

The conduction losses in this and the pervious interval $(0 < t < t_1)$ in both M_2 and D_3 are considered here together. According to Equation-2.5 and 2.9 respectively, these power losses can be obtained as shown:

$$\overline{P}_{M2on} = \frac{t_1 + t_2}{3T} I_{A\max}{}^2 R_{M2on} \tag{4.19}$$

$$\overline{P}_{D3on} = \frac{V_{D3} I_{A\max} (t_1 + t_2)}{2T} \tag{4.20}$$

c. At the beginning of this interval $(t_1 + t_2 < t < t_1 + t_2 + t_3)$, resonant inductor current i_{L2} is larger than main inductor current i_{L1}, and the body diode (not shown in Figure-4.6) of M_1 turns on to conduct the difference of the two currents. Also at the beginning the interval, M_1 is turned on (ZVS), and concurrently M_2 is turned off. With M_2 off, auxiliary diode D_2 is kicked in immediately. Following this, the resonant inductor current is completely reset, and consequently D_2 turns off.

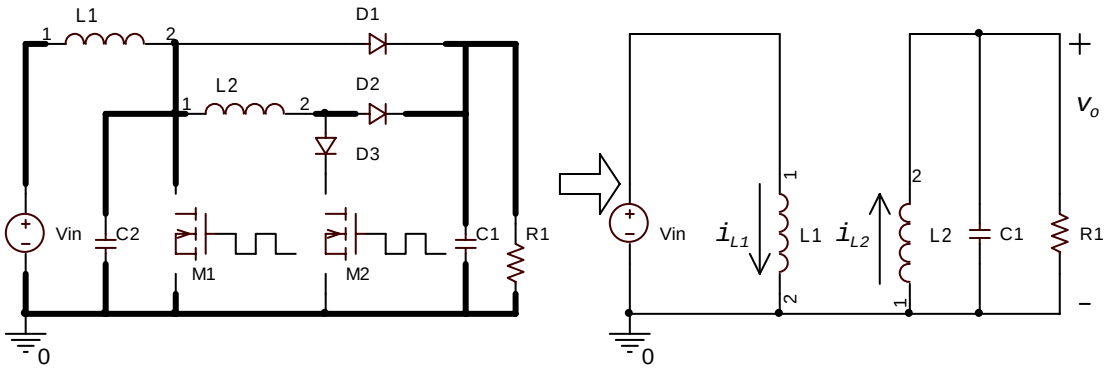

Figure-4.6 Ideal equivalent topology when M_1 and D_2 are on

All voltages and currents are defined according to the sign convention. KVL & KCL are expressed as:

$$-V_{in} + L_1 \frac{di_{L1}}{dt} = 0 \tag{4.21}$$

$$L_2 \frac{di_{L2}}{dt} + V_{C1} = 0 \tag{4.22}$$

$$i_{L2} - C_1 \frac{dv_{C1}}{dt} - \frac{v_{C1}}{R_1} = 0 \tag{4.23}$$

In the matrix form for the above equations:

$$\begin{bmatrix} \frac{di_{L1}}{dt} \\ \frac{di_{L2}}{dt} \\ \frac{dv_{C1}}{dt} \\ \frac{dv_{C2}}{dt} \end{bmatrix} = \begin{bmatrix} 0 & 0 & 0 & 0 \\ 0 & 0 & \frac{-1}{L_2} & 0 \\ 0 & \frac{1}{C_1} & \frac{-1}{R_1 C_1} & 0 \\ 0 & 0 & 0 & 0 \end{bmatrix} \begin{bmatrix} i_{L1} \\ i_{L2} \\ v_{C1} \\ v_{C2} \end{bmatrix} + \begin{bmatrix} \frac{V_{in}}{L_1} \\ 0 \\ 0 \\ 0 \end{bmatrix} \tag{4.24}$$

For the power analysis, only steady state is considered. In other words, V_o is equal to V_{C1} and is considered constant. It is only necessary to calculate both inductor-current i_{L1} and i_{L2} to obtain power losses. From Equation-4.21 and 4.22 inductor currents are obtained as shown:

$$\begin{cases} i_{L1} = \frac{V_{in}}{L_1}\left[t - (t_1 + t_2)\right] + i_{L1}\big|_{t1+t2} \\ i_{L2} = -\frac{V_o}{L_2}\left[t - (t_1 + t_2)\right] + I_{A\max} \end{cases}, \text{ where } (t_1 + t_2 < t < t_1 + t_2 + t_3) \tag{4.25}$$

$\because i_{L2}\big|_{t1+t2+t3} = 0$

$$\therefore t_3 = \frac{L_2 I_{A\max}}{V_o} \tag{4.26}$$

$$i_{L1}\big|_{t1+t2+t3} = \frac{V_{in} t_3}{L_1} + i_{L1}\big|_{t1+t2} = \frac{V_{in} L_2 I_{A\max}}{V_o L_1} + i_{L1}\big|_{t1+t2} \tag{4.27}$$

The resulting power losses in this interval include conduction loss in main MOSFET M_1 and auxiliary diode D_2, and turn-off loss in auxiliary MOSFET M_2. Turn-off loss $\left(\overline{P}_{M2turn-off}\right)$ in M_2 and conduction loss $\left(\overline{P}_{D2on}\right)$ in D_2.are calculated here. According to Equation-3.4, 3.7 respectively, $\overline{P}_{M2turn-off}$ and $\overline{P}_{D2on}$ can be obtained as shown:

$$\overline{P}_{M2turn-off} = \frac{V_o I_{A\max}^{\ 2}}{6kT} \tag{4.28}$$

$$\overline{P}_{D2on} = \frac{V_{D2} I_{A\max} t_3}{2T} \tag{4.29}$$

For simplicity the conduction loss for this interval in main MOSFET M_1 will be considered in the subsequent intervals.

d. In this interval $\left(t_1 + t_2 + t_3 < t < t_1 + t_2 + t_3 + t_4\right)$, main inductor L_1 is charged while main MOSFET M_1 is still on and the rest of semiconductor devices are off. This interval is identical to its hard switching counterpart.

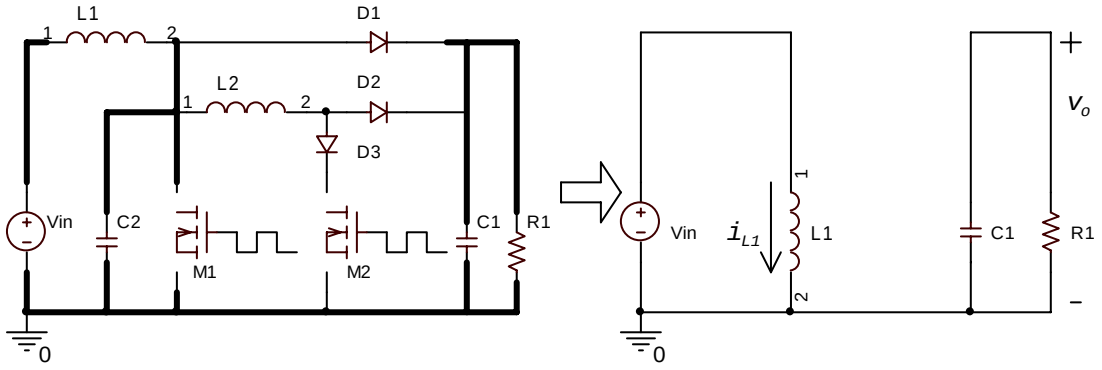

Figure-4.7 Ideal equivalent circuit when M_1 is on and other switches are off

All voltages and currents are defined according to the sign convention. KVL & KCL are expressed as:

$$-V_{in} + L_1 \frac{di_{L1}}{dt} = 0 \tag{4.30}$$

$$-C_1 \frac{dv_{C1}}{dt} - \frac{v_{C1}}{R_1} = 0 \tag{4.31}$$

In the matrix form for the above equations:

$$\begin{bmatrix} \frac{di_{L1}}{dt} \\ \frac{di_{L2}}{dt} \\ \frac{dv_{C1}}{dt} \\ \frac{dv_{C2}}{dt} \end{bmatrix} = \begin{bmatrix} 0 & 0 & 0 & 0 \\ 0 & 0 & 0 & 0 \\ 0 & 0 & \frac{-1}{R_1 C_1} & 0 \\ 0 & 0 & 0 & 0 \end{bmatrix} \begin{bmatrix} i_{L1} \\ i_{L2} \\ v_{C1} \\ v_{C2} \end{bmatrix} + \begin{bmatrix} \frac{V_{in}}{L_1} \\ 0 \\ 0 \\ 0 \end{bmatrix} \tag{4.32}$$

For the power analysis, only steady state is considered. In other words, V_o is equal to V_{C1} and is considered constant. It is only necessary to calculate main

inductor-current i_{L1} to obtain power losses. From equation 4.30, i_{L1} is obtained as shown:

$$i_{L1} = \frac{V_{in}}{L_1}\left[t - \left(t_1 + t_2 + t_3\right)\right] + i_{L1}\big|_{t1+t2+t3} ,$$

where $\left(t_1 + t_2 + t_3 < t < t_1 + t_2 + t_3 + t_4\right)$ (4.33)

From Figure-4.3:

$$DT = t_1 + t_2 + t_3 + t_4$$

$$\therefore t_4 = DT - \left(t_1 + t_2 + t_3\right), \text{ where D: duty cycle; T: period} \quad (4.34)$$

$$i_{L1}\big|_{t1+t2+t3+t4} = \frac{V_{in} t_4}{L_1} + i_{L1}\big|_{t1+t2+t3} \quad (4.35)$$

In this interval the only involved power loss is part of the conduction loss in main MOSFET M_1; which for simplicity is combined in calculations with the other part of this loss from the pervious interval $\left(t_1 + t_2 < t < t_1 + t_2 + t_3\right)$. According to Equation-3.5, the total conduction loss can be obtained as shown:

$$P_{M1on} = \frac{t_3 R_{Mon}\left(i_{L1}\big|_{t1+t2+t3}\right)^2}{3T}$$

$$+ \frac{t_4 R_{Mon}\left[\left(i_{L1}\big|_{t1+t2+t3}\right)^2 + \left(i_{L1}\big|_{t1+t2+t3}\right)\left(i_{L1}\big|_{t1+t2+t3+t4}\right) + \left(i_{L1}\big|_{t1+t2+t3+t4}\right)^2\right]}{3T} \quad (4.36)$$

e. At the start of this interval $\left(t_1 + t_2 + t_3 + t_4 < t < t_1 + t_2 + t_3 + t_4 + t_5\right)$, main MOSFET M_1 is turned off while other semiconductor devices are off. Subsequent to switching off M_1, main inductor L_1 starts to charge resonant capacitor C_2 which will eventually result in gradual turn-on of main diode D_1 in

the next interval. Although during the turn-off, drain voltage and current coexist in main MOSFET M_1, this energy is stored in the parasitic capacitor of the MOSFET and resonant capacitor C_2. It is noted that this energy is not consumed by main MOSFET M_1 and is transferred to the output capacitor in the next cycle with the help of the active snubber circuit. Therefore, there is no power losses involved in this interval. Moreover, the reverse voltage of main diode D_1 slowly decreases while the voltage of resonant capacitor C_2 increases, which leads to soft turn-on of D_1 in the next interval.

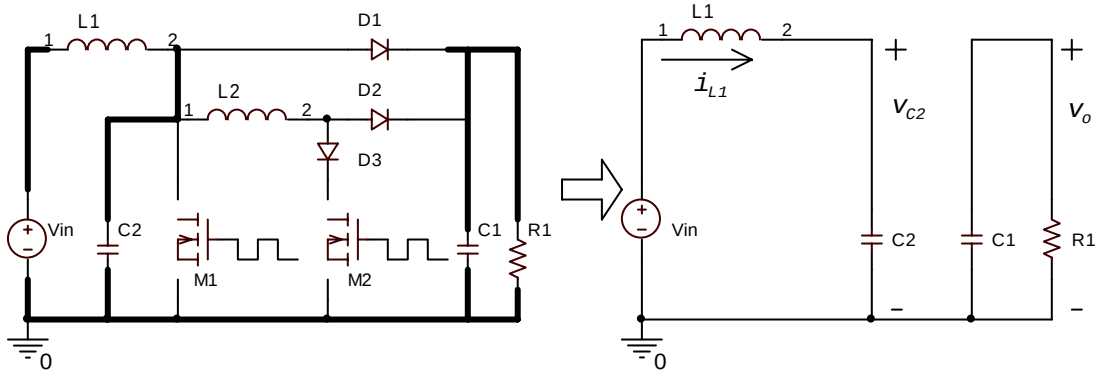

Figure-4.8 Ideal equivalent circuit when all switches are off

All voltages and currents are defined according to the sign convention. KVL & KCL are expressed as:

$$-V_{in} + L_1 \frac{di_{L1}}{dt} + V_{C2} = 0 \tag{4.37}$$

$$-C_1 \frac{dv_{C1}}{dt} - \frac{v_{C1}}{R_1} = 0 \tag{4.38}$$

$$i_{L1} - C_2 \frac{dv_{C2}}{dt} = 0 \tag{4.39}$$

In the matrix form for the above equations:

$$\begin{bmatrix} \frac{di_{L1}}{dt} \\ \frac{di_{L2}}{dt} \\ \frac{dv_{C1}}{dt} \\ \frac{dv_{C2}}{dt} \end{bmatrix} = \begin{bmatrix} 0 & 0 & 0 & \frac{-1}{L_1} \\ 0 & 0 & 0 & 0 \\ 0 & 0 & \frac{-1}{R_1 C_1} & 0 \\ \frac{1}{C_2} & 0 & 0 & 0 \end{bmatrix} \begin{bmatrix} i_{L1} \\ i_{L2} \\ v_{C1} \\ v_{C2} \end{bmatrix} + \begin{bmatrix} \frac{V_{in}}{L_1} \\ 0 \\ 0 \\ 0 \end{bmatrix} \tag{4.40}$$

Even though there are no power losses involved in this interval, main inductor current i_{L1} still needs to be calculated to obtain the input power. As mentioned before, in practice C_2 is selected to be around 500pF. Also L_1 is very large and can be considered as a constant current source in analyzing the circuit. That is, the main inductor current charges resonant capacitor C_2, and the energy stored in C_2 will be transferred to the resonant inductor in the next cycle (interval b). The interval time t_5 is calculated as follows:

$$\because V_{C2} = \frac{i_{L1}\big|_{t1+t2+t3+t4}}{C_2}\left[t - (t_1 + t_2 + t_3 + t_4)\right]$$

$$Also, \because V_{C2}\big|_{t_1+t_2+t_3+t_4+t_5} = V_o$$

$$\therefore t_5 = \frac{C_2 V_o}{i_{L1}\big|_{t1+t2+t3+t4}} \tag{4.41}$$

$$i_{L1}\big|_{t1+t2+t3+t4+t5} = i_{L1}\big|_{t1+t2+t3+t4} \tag{4.42}$$

f. At the start of this interval $(t_1 + t_2 + t_3 + t_4 + t_5 < t < t_1 + t_2 + t_3 + t_4 + t_5 + t_6)$, main diode D_1 is turned on (soft turn-on) and thus main inductor L_1 starts to charge output capacitor C_1 in the same manner as its hard switching counterpart. In this

interval the only involved power loss is part of the conduction loss in main diode D_1; which for simplicity is combined in calculations with the other part of this loss from interval $(0 < t < t_1)$.

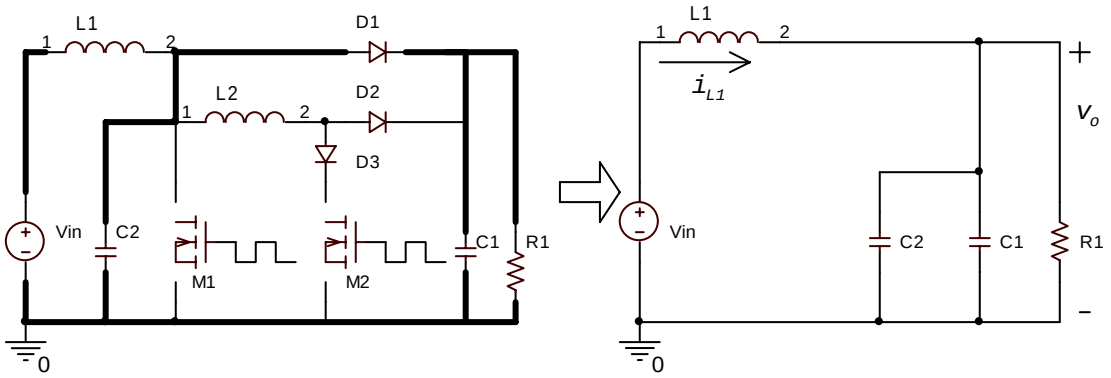

Figure-4.9 Main diode on and ideal equivalent circuit

All voltages and currents are defined according to the sign convention. KVL & KCL are expressed as:

$$-V_{in} + L_1 \frac{di_{L1}}{dt} + V_{C1} = 0 \tag{4.43}$$

$$i_{L1} - (C_1 + C_2)\frac{dv_{C1}}{dt} - \frac{v_{C1}}{R_1} = 0 \tag{4.44}$$

$$i_{L1} - (C_1 + C_2)\frac{dv_{C2}}{dt} - \frac{v_{C2}}{R_1} = 0 \tag{4.45}$$

In the matrix form for the above equations:

$$\begin{bmatrix} \frac{di_{L1}}{dt} \\ \frac{di_{L2}}{dt} \\ \frac{dv_{C1}}{dt} \\ \frac{dv_{C2}}{dt} \end{bmatrix} = \begin{bmatrix} 0 & 0 & \frac{-1}{L_1} & 0 \\ 0 & 0 & 0 & 0 \\ \frac{1}{C_1+C_2} & 0 & \frac{-1}{R_1(C_1+C_2)} & 0 \\ \frac{1}{C_1+C_2} & 0 & 0 & \frac{-1}{R_1(C_1+C_2)} \end{bmatrix} \begin{bmatrix} i_{L1} \\ i_{L2} \\ v_{C1} \\ v_{C2} \end{bmatrix} + \begin{bmatrix} \frac{V_{in}}{L_1} \\ 0 \\ 0 \\ 0 \end{bmatrix} \quad (4.46)$$

For the power analysis, only steady state is considered. In other words, V_o is equal to V_{C1} and is considered constant. It is only necessary to calculate main inductor-current i_{L1} to obtain power losses in this interval. From Equation-4.33, i_{L1} is obtained as shown:

$$i_{L1} = \frac{V_{in} - V_o}{L_1}\left[t - (t_1 + t_2 + t_3 + t_4 + t_5)\right] + i_{L1}\big|_{t1+t2+t3+t4+t5},$$

where $(t_1 + t_2 + t_3 + t_4 + t_5 < t < t_1 + t_2 + t_3 + t_4 + t_5 + t_6 = T)$ (4.47)

$$i_{L1}\big|_T = \frac{V_{in} - V_o}{L_1} t_6 + i_{L1}\big|_{t1+t2+t3+t4+t5} \quad (4.48)$$

From Figure-4.3:

$T = DT + t_5 + t_6$

$\therefore t_6 = T - (DT + t_5)$, where D: duty cycle; T: period (4.49)

According to Equation-2.10, the total conduction loss can be obtained as shown:

$$\overline{P}_{D1on} = \frac{V_{D1}\left(i_{L1}\big|_{t1+t2+t3+t4+t5} + i_{L1}\big|_T\right)t_6}{2T} + \frac{V_{D1} i_{L1}\big|_T t_1}{2T} \quad (4.50)$$

4.4 Obtaining duty cycle and average inductor current for power analysis

It is necessary to obtain the duty cycle and average main inductor current ($\overline{i_{L1}}$) as necessary parameters for power analysis. $\overline{i_{L1}}$ is needed to obtain the input power and duty cycle (D) is required to obtain minimum and maximum main inductor currents. Now $\overline{i_{L1}}$ is calculated by taking the time average of main inductor currents in each of the intervals indicated in the above section. Approximations are made for the minimum and maximum main inductor currents ($I_{L1\min}$ and $I_{L1\max}$) according to the relevant expressions for i_{L1} in each interval:

1. the minimum inductor current, $I_{L1\min} \approx i_{L1}\big|_{t1}$ (4.51)
2. the maximum inductor current, $I_{L1\max} \approx i_{L1}\big|_{t1+t2+t3+t4}$ (4.52)

Finally average main inductor current can be obtained as follows:

$$\overline{i_{L1}} \approx \frac{i_{L1}\big|_{t1} + i_{L1}\big|_{t1+t2+t3+t4}}{2} \tag{4.53}$$

Also from the continuous current assumption:

$$i_{L1}\big|_{T} = i_{L1}\big|_{0} \neq 0 \tag{4.54}$$

Power balance equation is given by:

$$V_{in}\overline{i_{L1}} = \frac{V_o^{\,2}}{R_1} + \overline{P}_{M2turnon} + \overline{P}_{M2turnoff} + \overline{P}_{M2on} + \overline{P}_{D2switching} + \overline{P}_{D2on} + \overline{P}_{D3on} + \overline{P}_{M1on} + \overline{P}_{D1on}$$

(4.55)

4.5 A method to calculate duty cycle and minimum and maximum inductor currents (D, I_{L1min}, I_{L1max})

The aim of these calculations is to obtain the power losses in the semiconductor devices (MOSFETs and diodes). Numerical method is used in MATLAB for this purpose in order to take advantage of the computer's utility. First guess value is used for $i_{L1}\big|_0$ in Equation-4.54 to obtain the duty cycle. At the same time $I_{L1\min}$ and $I_{L1\max}$ are obtained. At this point we have all the trial values for *D*, and $I_{L1\min}$ and $I_{L1\max}$ based on this the losses are calculated according to the respective equations stated above. Next these power loss values are continuously tested in the power balance Equation-4.55 and if this equation is satisfied then the solution is reached.

4.6 The analytical result and hardware-test result

For these calculations the following parameters were used:

$$\begin{cases} L_1 = 140uH \\ L_2 = 5.2uH \\ C_1 = 470uF \\ C_2 = 680\,pF \\ V_{in} = 60V \\ V_o = 200V \\ R_L = 66.5\Omega \end{cases} \qquad \begin{cases} k = 200A/us \\ I_{Arr} = 7.0A \\ t_{Arr} = 28ns \\ R_{Mon} = 76m\Omega \\ R_{Aon} = 120m\Omega \\ V_{D1,2,3} = 1.7V \end{cases} \tag{4.56}$$

$$\eta = \frac{\frac{V_o^{\,2}}{R_L}}{V_{in} I_{in}} \tag{4.57}$$

Figure-4.10 shows the total switching loss and conduction loss in semiconductor devices of soft-switching converter, obtained from the above analysis. As it is evident from the figure, conduction loss dominates the total losses. Lower frequencies correspond to higher current ripple in main inductor L_1 and visa versa. This is significant because rising component of the ripple also appears in main MOSFET M_1. This contributes to the conduction loss of M_1 which is proportion to square of the current through it (Equation-4.36). In other words, higher ripples mean higher power losses. At around 50Hz it is observed that the conduction loss starts to increase with increasing frequency. This is due to proportional relationship between conduction power losses of M_2, D_2, and D_3 and frequency, which is described in Equations-4.19, 4.20 and 4.29. The results from the hardware tests are summarized in Table-4.1. Efficiency of the system is calculated according to Equation-4.57. As it is evident from this equation, V_o, V_{in}, and R_L are all constants, and therefore I_{in} is the only parameter has an influence on the efficiency. Figure-4.11 shows the efficiencies of both hard-switching and soft-switching converters, which are obtained from the analytic methods and hardware tests.

Table-4.1 Input current versus operating frequency (hardware test)

f (kHz)	25.0	51	76	102	127	147	175	201	222	249	276
I_{in}.(A)	10.09	10.09	10.15	10.22	10.28	10.32	10.36	10.42	10.48	10.55	10.65
η (%)	99.36	99.36	98.77	98.09	97.52	97.14	96.77	96.21	95.66	95.02	94.13

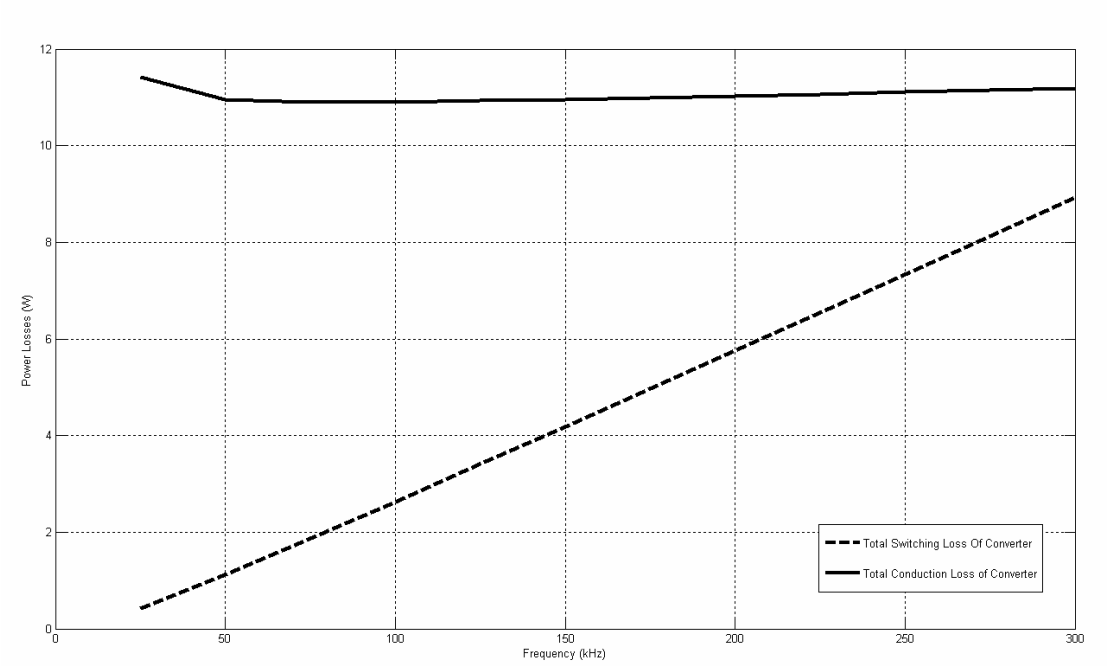

Figure-4.10 Total switching and conduction losses versus frequency

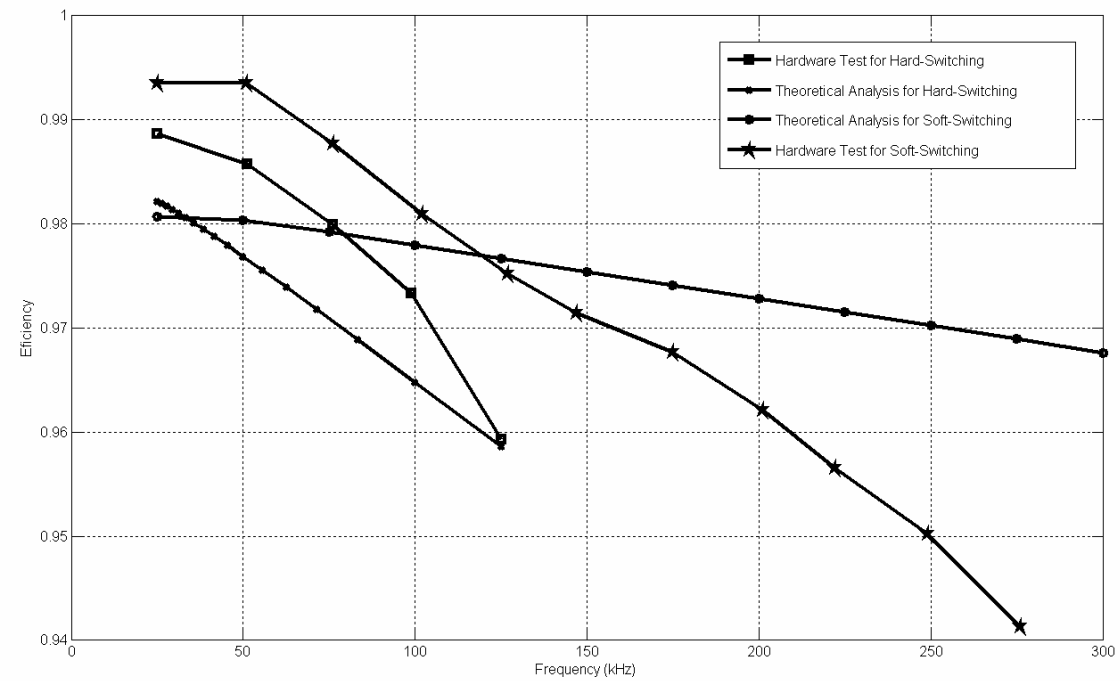

Figure-4.11 Efficiencies obtained from analysis and hardware tests versus frequency

The following discussion refers to Figure-4.11. As it is shown, at very low frequencies (less than 30 kHz) the efficiency of soft-switching converter is lower than its hard-switching counterpart from the analytic method. This is because conduction losses at this frequency range dominate the total losses and since the soft-switching converter has additional semiconductor devices, these contribute to more losses. In the case of soft-switching, an error is observed between the efficiencies obtained from theoretical analysis and hardware tests. This can be explained by omission of losses in the resonant capacitor and inductor in our model. As it is depicted in Figure-4.12, high values of capacitor-and-inductor temperatures are measured at higher frequencies which represent higher losses. As mentioned before oscillations in M_2 and L_2 loop also contribute to these losses which were not considered in the model. Based on the information represented in the above graphs and equations, a designer is able to estimate losses for each of the semiconductor devices. Also this information can be used in selecting a heat sink with an appropriate thermal resistance so as to avoid crossing the maximum allowed junction temperature.

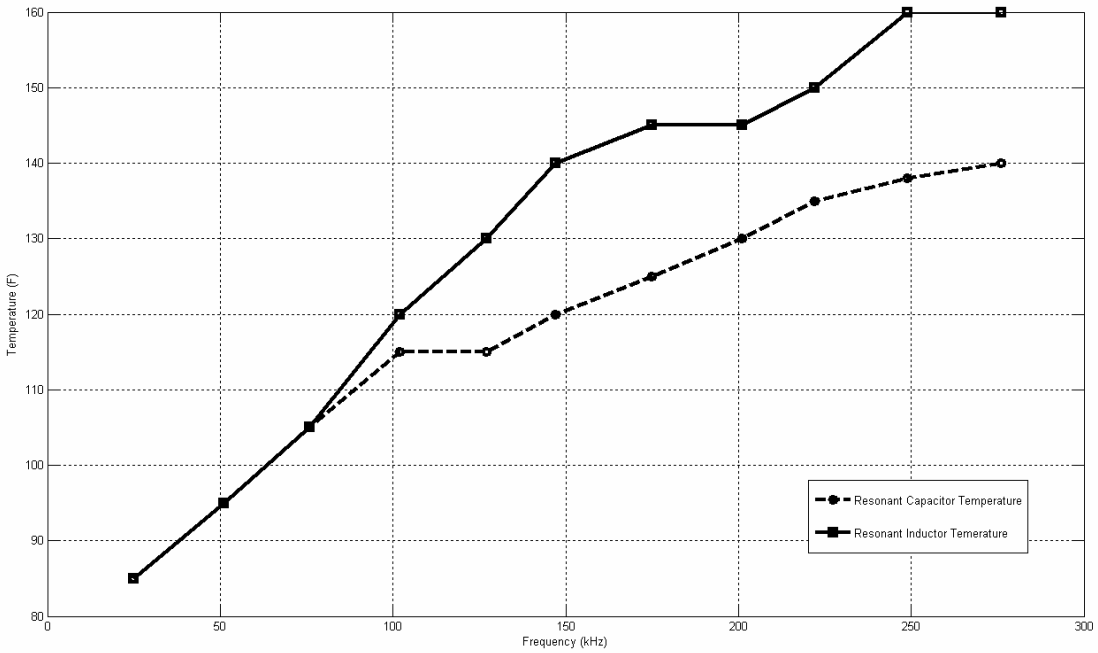

Figure-4.12 Resonant capacitor and inductor temperature versus frequency (ambient temperature at 70 F)

CHAPTER 5

CONTROL SYSTEM DESIGN AND HARDWARE IMPLEMATATION

5.1 Feedback for power electronics converters

Regulation is one of the key attributes of power supplies. Regulation in power electronics converters refers to controlling of output voltage, current, or power so that the output is held within the allowed tolerance. This control action is necessary because certain disturbances exist in the input voltage and the output loading for different applications.[37] Also component values such as those of capacitors can change over time and consequently change the dynamics of the converter. Therefore, it is necessary to utilize a controller so that the output parameter is not affected (within a tolerance) by the disturbances and the parametric drifts. Control of a power supply is normally accomplished by using a negative-feedback control system, where output parameter is sensed and compared to a reference value (desired value of output parameter). Difference between these two values (sensed and desired values) constitutes the error which will be the input to the controller. Also a feed forward can be used to further enhance the output of the system. One way that feed forward accomplishes this is by sensing the input and taking a corrective action before the effect appears at the output.

Usually in order to design a controller for a certain system (plant), either a mathematical model or experimentally determined frequency response of the system is necessary.[38] In power supply design, the dynamic equations can be obtained fairly

easily by making certain assumptions, such as ideal semiconductor devices (either completely on or off). This appears in the form of several sets of differential equations (one set for each switching interval) that can also be represented in state-space form.[39] Initial conditions for these DEQs come from boundary conditions that exist at the instances of switching actions.[40] PWM converters belong to a class of time variant non-linear systems where the system is sequentially switched between several linear-systems.[39] For example, the resonant converter described in this thesis is switched between six intervals. Clearly this system does not meet the definition of a time-invariant linear system. Most of the familiar control techniques such as root locus and Nyquist stability criterion can only be applied to time-invariant linear systems. Therefore after obtaining the dynamic model (DEQs of the system) the next step is to attempt to linearize this model in order to take advantage the mentioned control techniques.

A state-space averaging technique was developed by Middlebrook and Cuk[39] that has been successfully used in linearizing switched mode converters. Mathematical justification of this model is lengthy, and therefore it will not be discussed here. But the general approach consists of introducing a switching function (equal to either 1 or 0 at different intervals) into our dynamic model so that several sets of DFQs are reduced to one set of DFQs equation. Then when taking Laplace transform of the resulted DFQs, we only use the first two terms of the tailor series expansion of the switching function. Finally this will yield the averaging model which is simply taking the time averages of matrices A, B, C, and D in the state-space representation.

One last step remains from obtaining the transfer function of the system. After obtaining the average state-space model we note that in most cases the control-signal (duty cycle) appears in a product term with a state variable. Multiplication of a duty ratio and state variable results in a non-linearity since both are functions of time. This will make the average model nonlinear. Also, sometimes, as in Boost converter, the relationship between duty cycle and output is not a linear mapping. Therefore, small-signal restriction becomes necessary in order to linearize these equations. Small signal analysis is employed to describe the system for small variations around a well defined operating point. Summery of steps required to derive the transfer function from dynamic model of a converter is listed below:

1. Obtain a state-space representation of the system from the respective sets of DFQs.
2. Obtain a state-space average model by taking the time average of A, B, C, and D in the state-space representation.
3. Linearize state-space average model obtained in step 2 in order to use frequency domain control methods.
4. Drive the transfer function.

5.2 Fuel cell system model

Steady-state and transient output characteristics of a typical PEM fuel cell system (Nexa™) were examined in Chapter-2 and now will be used for the purpose of control design. The results from this study are used to derive a fuel cell model that

adequately emulates the electrical response of the fuel cell system under the load dynamics of interest. It was concluded in Chapter-2 that at frequencies above 500 Hz, the response time approaches zero. Therefore, the high frequency current ripple (caused by switching action) will not have a significant effect on the fuel cell system's output. On the other hand the low frequency ripple has negative impact on the performance, efficiency, power capacity, and lifetime of the fuel cell system. For this reason the low frequency ripple current has to be avoided at the output of the fuel cell. This is accomplished by utilizing a control scheme that limits the low frequency current ripple. With these assumptions, the fuel cell system can be modeled as an ideal source with a series resistance that can be calculated according to Figure-2.4 (R=0.23).

5.3 State-space averaging model

In Chapter-4, state-space representations were presented for all six switching intervals within a cycle. In this chapter these results will be used in order to derive the state-space averaging model. The converter comprises of four energy storage components. Therefore, minimum number of four state variables ($i_{L1}, i_{L2}, v_{C1}, v_{C2}$) are necessary to completely describe the system (assuming ideal switches). This allows us to consider the converter as consisting of a two-port device that represents the nonlinear time-variant (NLTV) part, depicted in Figure-5.1.

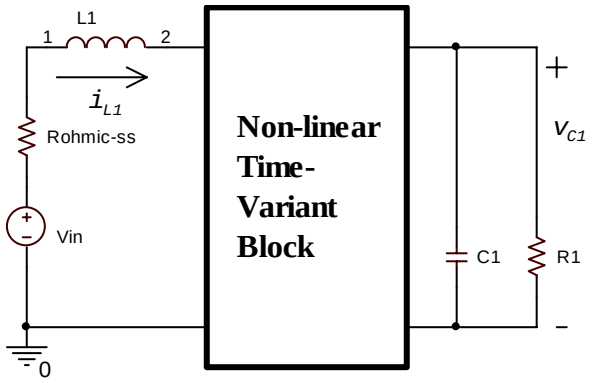

Figure-5.1 System description of soft switching boost converter

Input state equation and output state equations of NLTV block can describe the system dynamics and steady-state characteristics of the converter. Therefore, in designing a controller to regulate the output voltage $y = v_{C1}$, we only need to consider $x_1 = i_{L1}$ and $x_2 = v_{C1}$.

According to Figure-4.3 each cycle consists of six intervals. By examining the state equations for each interval it is observed that intervals t_1 and t_6 can be described by same state equations and the same is true about t_3 and t_4. Because the switching action is periodic, intervals t_1 and neighboring t_6 can be considered as one interval. This will make t_2 the beginning of the period and t_1 the end of the period. Therefore, duty cycle d in this chapter is redefined as $\frac{t_2 + t_3 + t_4}{T}$ which implies $(1-d) = \frac{t_5 + t_6 + t_1}{T}$. From Equations-4.18 and 4.41, t_2 and t_5 are small relative to the switching period. During this time (t_2 and t_5), inductor current ($x_1 = i_{L1}$) and output voltage ($x_2 = v_{C1}$) do not change considerably. Therefore state equations for intervals t_2 and t_5 can be replaced

(approximated) by state equations for intervals t_3 and t_6 respectively. This process will result in two intervals with corresponding state space equations, shown below:

a. During dT, the state equations are rewritten the blow from Equation-4.30, 4.31:

$$-V_{in} + R_{ss} i_{L1} + L_1 \frac{di_{L1}}{dt} = 0 \tag{5.1}$$

$$-C_1 \frac{dv_{C1}}{dt} - \frac{v_{C1}}{R_1} = 0 \tag{5.2}$$

In the matrix form for the above equations:

$$\begin{bmatrix} \dot{x}_1 \\ \dot{x}_2 \end{bmatrix} = \begin{bmatrix} \frac{-R_{ss}}{L_1} & 0 \\ 0 & \frac{-1}{R_1 C_1} \end{bmatrix} \begin{bmatrix} x_1 \\ x_2 \end{bmatrix} + \begin{bmatrix} \frac{V_{in}}{L_1} \\ 0 \end{bmatrix} \tag{5.3}$$

$$A_1 = \begin{bmatrix} \frac{-R_{ss}}{L_1} & 0 \\ 0 & \frac{-1}{R_1 C_1} \end{bmatrix},\ B_{V1} = \begin{bmatrix} \frac{V_{in}}{L_1} \\ 0 \end{bmatrix},\ C_1^T = \begin{bmatrix} 0 & 1 \end{bmatrix} \tag{5.4}$$

b. During $(1-d)T$, the state equations are written the below from Equation-4.43, 4.44:

$$-V_{in} + R_{ss} i_{L1} + L_1 \frac{di_{L1}}{dt} + V_{C1} = 0 \tag{5.5}$$

$$i_{L1} - (C_1 + C_2)\frac{dv_{C1}}{dt} - \frac{v_{C1}}{R_1} = 0 \tag{5.6}$$

In the matrix form for the above equations:

$$\begin{bmatrix} \dot{x}_1 \\ \\ \dot{x}_2 \end{bmatrix} = \begin{bmatrix} \dfrac{-R_{ss}}{L_1} & \dfrac{-1}{L_1} \\ \dfrac{1}{C_1} & \dfrac{-1}{R_1 C_1} \end{bmatrix} \begin{bmatrix} x_1 \\ \\ x_2 \end{bmatrix} + \begin{bmatrix} \dfrac{V_{in}}{L_1} \\ \\ 0 \end{bmatrix} \tag{5.7}$$

$$A_2 = \begin{bmatrix} \dfrac{-R_{ss}}{L_1} & \dfrac{-1}{L_1} \\ \dfrac{1}{C_1} & \dfrac{-1}{R_1 C_1} \end{bmatrix},\ B_{V2} = \begin{bmatrix} \dfrac{V_{in}}{L_1} \\ \\ 0 \end{bmatrix},\ C_2^T = \begin{bmatrix} 0 & 1 \end{bmatrix} \tag{5.8}$$

Average state-variable description of the system is given by:[41]

$$A = A_1 \cdot d + A_2 \cdot (1-d)$$

$$B_V = B_{V1} \cdot d + B_{V2} \cdot (1-d)$$

$$C^T = C_1^T \cdot d + C_2^T \cdot (1-d)$$

$$\begin{bmatrix} \dot{x}_1 \\ \\ \dot{x}_2 \end{bmatrix} = \begin{bmatrix} \dfrac{-R_{ss}}{L_1} & -\dfrac{(1-d)}{L_1} \\ \dfrac{(1-d)}{C_1} & \dfrac{-1}{R_1 C_1} \end{bmatrix} \begin{bmatrix} x_1 \\ \\ x_2 \end{bmatrix} + \begin{bmatrix} \dfrac{V_{in}}{L_1} \\ \\ 0 \end{bmatrix} \tag{5.9}$$

For the controller design, output variables of interest are main inductor current and output voltage:

$$y_1 = x_1 \tag{5.10}$$

$$y_2 = x_2 \tag{5.11}$$

The above description captures information about the dc and low frequency characteristics of the converter, but it eliminates information about high frequency characteristics and other fast effects. Even though ripple is not given in the average output, and average model is still useful in determining both steady-state and dynamic

response of the system. We see that the above state equations are nonlinear with respect to duty cycle d. Therefore, $\dot{x} = f(x,d)$ and $y = h(x,d)$ have to be linearized. This is accomplished by obtaining the Jacobian matrices:

$$A(x,d) = \left[\frac{\partial f}{\partial x}\right],\ B(x,d) = \left[\frac{\partial f}{\partial d}\right], \text{ and } C(x,d) = \left[\frac{\partial h}{\partial x}\right] \tag{5.12}$$

$$A(x,d) = \begin{bmatrix} \frac{\partial f_1}{\partial x_1} & \frac{\partial f_1}{\partial x_2} \\ \frac{\partial f_2}{\partial x_1} & \frac{\partial f_2}{\partial x_2} \end{bmatrix} = \begin{bmatrix} \frac{-R_{ss}}{L_1} & -\frac{(1-d)}{L_1} \\ \frac{(1-d)}{C_1} & -\frac{1}{R_1 C_1} \end{bmatrix} \underline{\underline{d = D}} \begin{bmatrix} -R_{ss} & -\frac{(1-D)}{L_1} \\ \frac{(1-D)}{C_1} & -\frac{1}{R_1 C_1} \end{bmatrix} \tag{5.13}$$

$$B(x,d) = \begin{bmatrix} \frac{\partial f_1}{\partial d} \\ \frac{\partial f_2}{\partial d} \end{bmatrix} = \begin{bmatrix} \frac{x_2}{L_1} \\ -\frac{x_1}{C_1} \end{bmatrix} \underline{\underline{\begin{matrix} x_1 = I_{L1} \\ x_2 = V_{C1} \end{matrix}}} \begin{bmatrix} \frac{V_{C1}}{L_1} \\ -\frac{I_{L1}}{C_1} \end{bmatrix} \tag{5.14}$$

$$C(x,d)^T = \begin{bmatrix} \frac{\partial h}{\partial x_1} & \frac{\partial f_2}{\partial x_2} \end{bmatrix} = \begin{bmatrix} 1 & 0 \end{bmatrix} \tag{5.15}$$

The above matrices are evaluated at an equilibrium point (X,D) to obtain system matrices A,B,C. This will result in a linear time-invariant approximation of the system which is valid for small signal around an equilibrium point symbolized by squiggly lines above the respective variables $\widetilde{I}_{L1}$, $\widetilde{d}$, and $\widetilde{v}_{c1}$.

Next step after linearizing the average-state-space representation is deriving transfer functions $\frac{\widetilde{I}_{L1}(s)}{\widetilde{d}(s)}$ and $\frac{\widetilde{v}_{C1}(s)}{\widetilde{I}_L(s)}$, which will be utilized in designing the controller to regulate the output voltage.

$$\frac{\widetilde{I}_{L1}(s)}{\widetilde{d}(s)} = C^T \cdot (s \cdot I - A)^{-1} \cdot B \tag{5.16}$$

$$\frac{\widetilde{I}_{L1}(s)}{\widetilde{d}(s)} = \begin{bmatrix} 1 & 0 \end{bmatrix} \cdot \begin{bmatrix} s + \frac{R_{ss}}{L_1} & \frac{(1-D)}{L_1} \\ -\frac{(1-D)}{C_1} & s + \frac{1}{R_1 C_1} \end{bmatrix}^{-1} \cdot \begin{bmatrix} \frac{V_{C1}}{L_1} \\ -\frac{I_{L1}}{C_1} \end{bmatrix}$$

$$\frac{\widetilde{I}_{L1}(s)}{\widetilde{d}(s)} = \frac{V_{C1} \cdot R_1 \cdot C_1 \cdot s + V_{C1} + R_1 \cdot I_{L1} \cdot (1-D)}{R_1 \cdot C_1 \cdot L_1 \cdot s^2 + (L_1 + R_{ss} \cdot R_1 \cdot C)s + R_{ss} + R_1 \cdot (1-D)^2} \tag{5.17}$$

Then from equation 5.9, $\frac{\widetilde{v}_{C1}(s)}{\widetilde{I}_L(s)}$ is given by:

$$\frac{\widetilde{v}_{C1}(s)}{\widetilde{I}_L(s)} = \frac{(1-D)/C_1}{s + 1/(C_1 \cdot R_1)} \tag{5.18}$$

5.4 Compensator design

In the pervious section a fuel cell model was used for the purpose of control design. As mentioned before, validity of this model depends on the ripple content of the fuel cell current. In order to enhance the performance and efficiency of the fuel cell system while satisfying the current ripple and power capacity requirements, low frequency current ripple needs to be avoided at the output. This can be achieved according to the following considerations.

1. Duel-loop controller will be designed with a current loop as the inner loop and a voltage loop as the output loop. The purpose of the additional current loop is to have a control over the speed at which the input current responds to control signal. The parameters of the current loop will be selected with the intention of

confining the input current to low frequencies, by making the response time of the controller sufficiently long. The slow response of the converter controller will provide sufficient time for the fuel cell control module to respond to changes in the load. This will ensure that the fuel cell system operates approximately on the steady state curve shown in Figure-2.4. Low frequency input current has the benefit of decreasing the capacitor effect and thereby simplifying the fuel cell model.

2. As mentioned before (Chapter-2), at high frequencies, rising and falling time constants of output fuel cell current appears to be zero. This implies that the switching action, that causes current ripple, will not have a significant transient response and only affects the steady state response. This further simplifies the fuel cell model by eliminating the need to model the transient response of fuel cell output current at high frequencies.
3. Transient load demands are supplied by an ultra capacitor (or backup battery at the output. Ultra capacitor design is beyond the scope of this thesis but it is an important component of most fuel cell applications that involve fast load dynamics, such as FC vehicles. Also because of fuel cell output limitations, the voltage controller discussed here is only responsible for responding to slow changes in the load.

Normal operating points and system parameters are given below:

$$\begin{cases} V_{C1} = 200V \\ I_{L1} = 10A \\ D = 0.7 \end{cases}$$

$$\begin{cases} L = 140\mu H \\ C_1 = 400\mu F \\ R_l = 66.5\Omega \\ R_{ss} = 0.23 \end{cases}$$

Simulink block diagram for disturbance test is provided below. Controller regulates the output voltage is two steps by utilizing a dual-loop scheme. The dual-loop controller consists of an output voltage loop and an inner current loop. The function of the outer voltage loop is to regulate the output voltage by adjusting the current reference in the current loop. The function of the inner current loop is to generate an appropriate duty ratio in order to control the inductor current. The Simulink block diagram of the controller action is provided below.

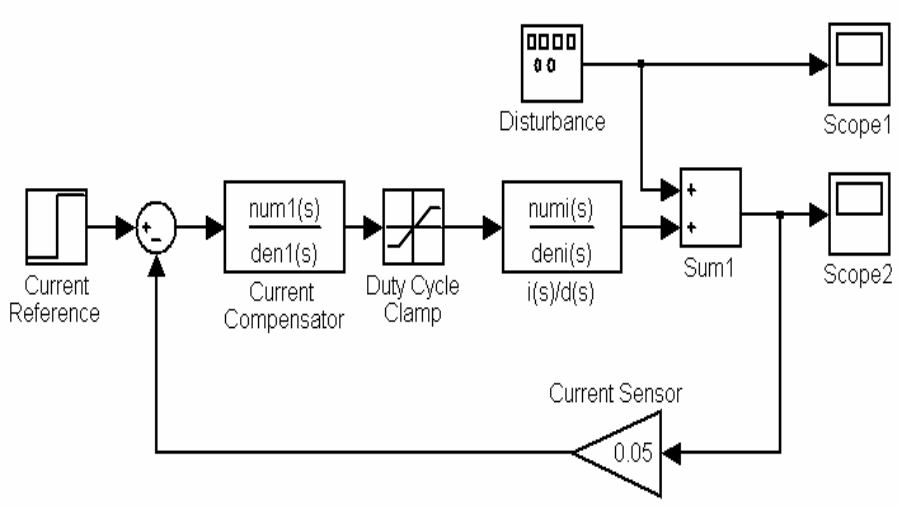

Figure-5.2 Simulink block diagram for inductor current compensator with disturbance

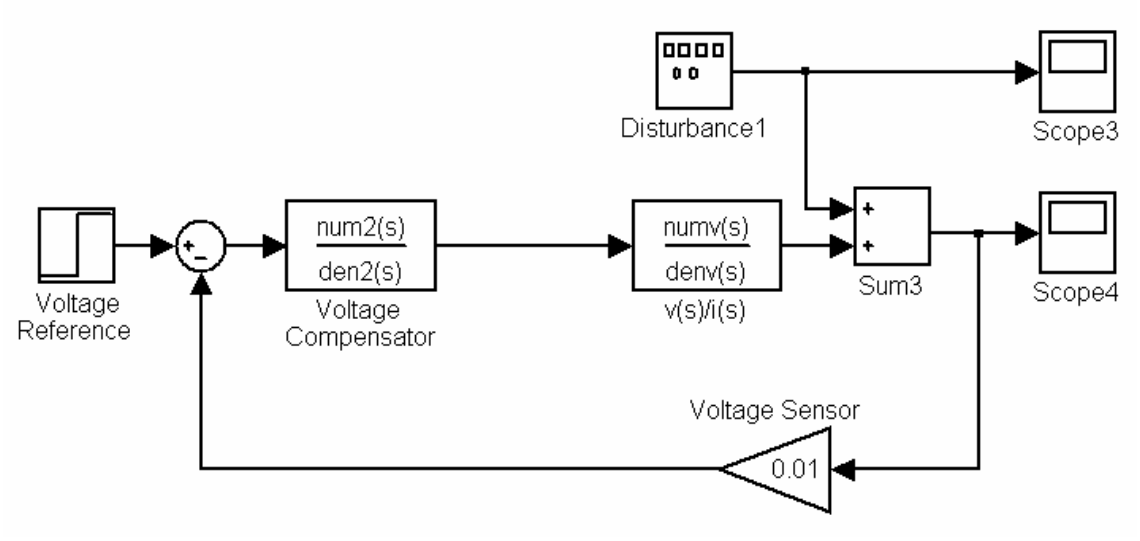

Figure-5.3 Simulink block diagram for output voltage compensator with disturbance

Frequency domain method such as bode plots were used to help in design of a controller. It is crucial to provide sufficient phase margin for stability. Another important criterion in frequency design is providing sufficient bandwidth in order to speed up the response of the system to disturbances. But, bandwidth can not be increased indefinitely because it will lead to noise amplification and thereby system will become unstable. Also here, limiting the bandwidth will serve another key objective which is to reduce the low frequency current ripple of the fuel cell system. In order to limit the low frequency current ripple the converter system bandwidth is confined less than 1 Hz. Some of the bode-plots used in the design process are provided below.

Figure-5.4 and Figure-5.6 show the bode-plots for closed loop gains with current loop and voltage loop respectively. Disturbances are simulated for the current loop (Figure-5.5), voltage loop (Figure-5.7), and the entire system (Figure-5.9) in order to verify the design.

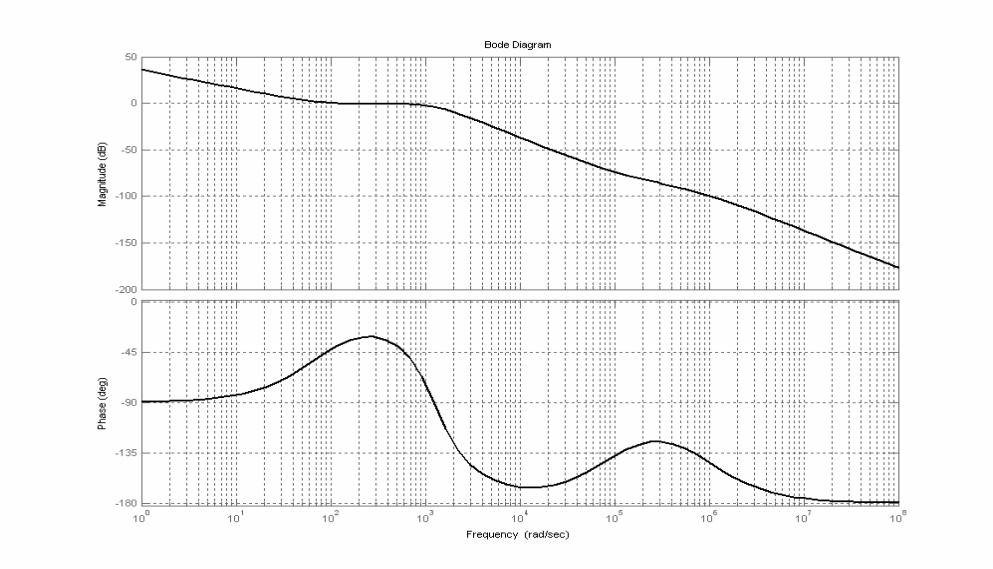

Figure-5.4 Bode plot for $\frac{\widetilde{I}_{L1}(s)}{\widetilde{d}(s)}$ with integral-lead compensator

The current loop performance was verified by applying a disturbance of 1 A (Figure-5.5). Current loop action prevents load variations to cross the current ripple limitation of the fuel cell system by responding with a proper delay.

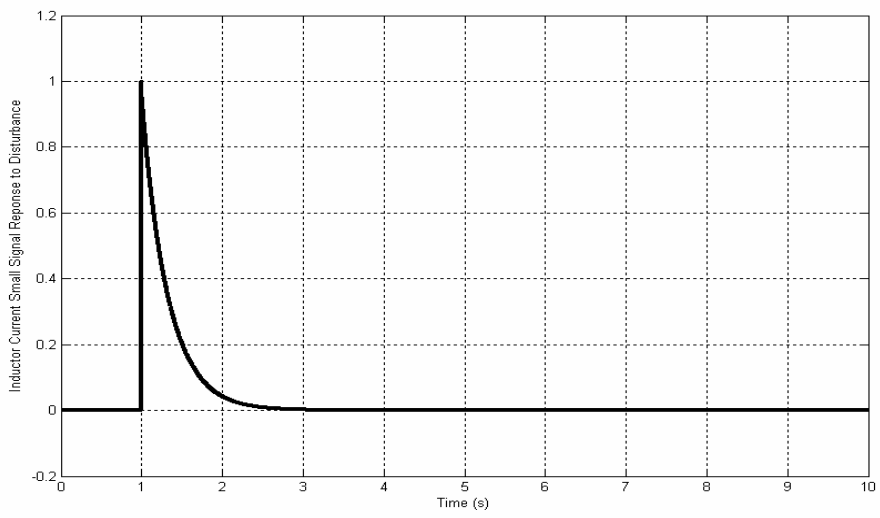

Figure-5.5 Inductor current response to step disturbance of 1 A

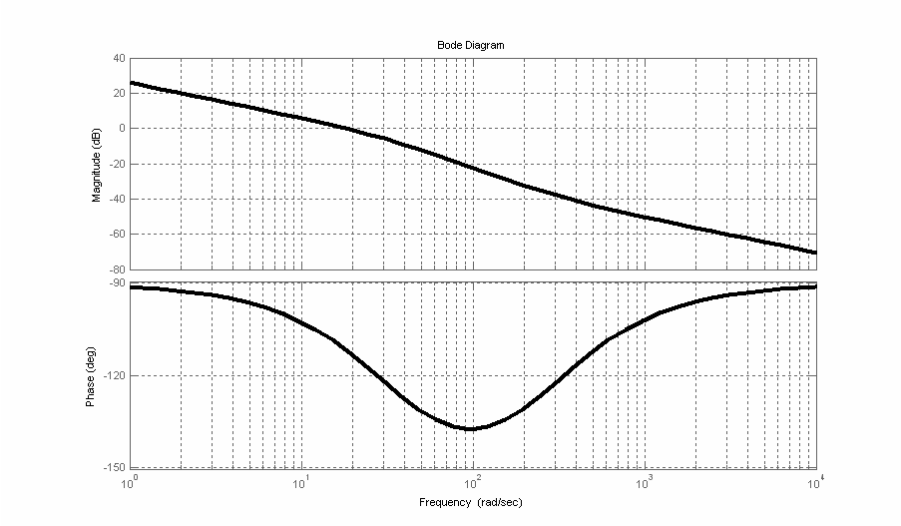

Figure-5.6 Bode plot for $\frac{\widetilde{v}_{C1}(s)}{\widetilde{I}_L(s)}$ with proportional-integral compensator

The voltage loop performance was verified using a disturbance of 20V (Figure-5.7). Voltage loop action prevents load variations to cross the current ripple limitation of the fuel cell system by responding with a proper delay.

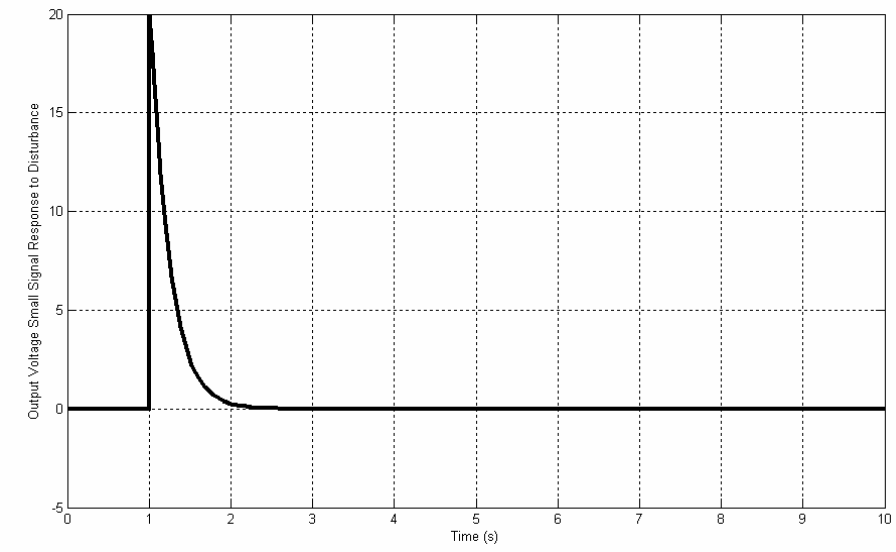

Figure-5.7 Output voltage small signal response to disturbance

Next the performance of the controller was tested with disturbance of 20V (Figure-5.8). Performance of dual loop was verified by applying a disturbance of 20V (Figure-5.9). Controller satisfied the Fuel cell current ripple requirement while meeting the stability criteria.

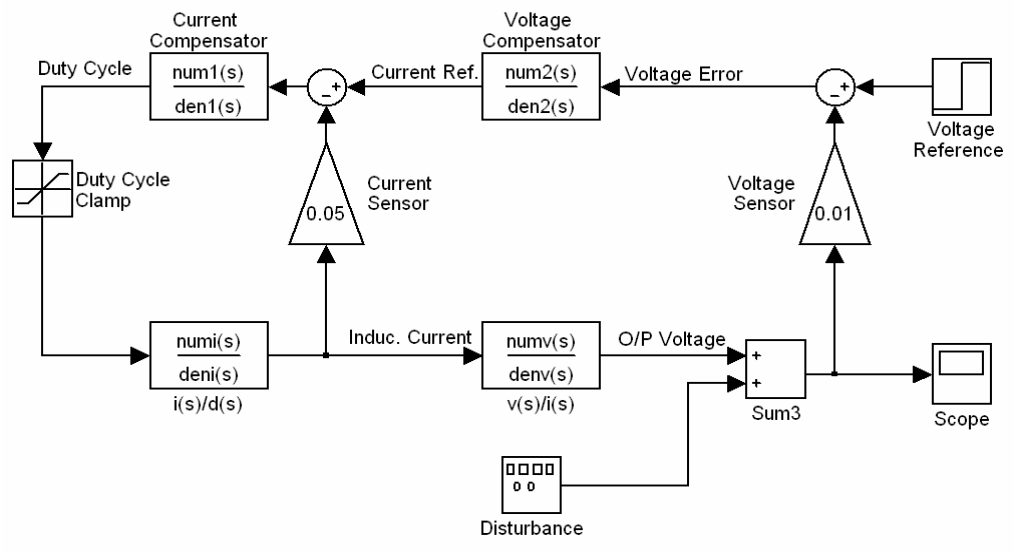

Figure-5.8 Simulink block diagram for whole system with disturbance

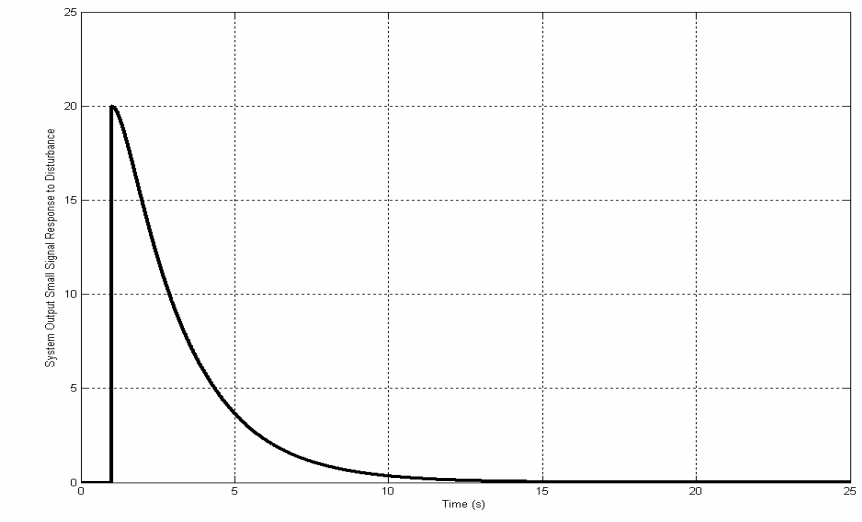

Figure-5.9 System output voltage small signal response to disturbance

Average state space model was derived for the converter and was used in frequency domain control design. State space averaging method provided a useful tool in designing a controller for the converter by making possible the utility of frequency domain control analysis. But the analysis with the average model eliminates some important information about the fast changing dynamics of the system which can not be represented in the above bode plots. Therefore, this model is only useful to analyze the behavior of the system in frequencies slower than the switching frequency. This has few implications in designing a controller for a practical application and therefore some considerations are necessary. Low-pass filter can be useful to reduce noise caused by switching frequency in feedback loop. Also phase margins in the above bode plots do not represent the actual phase margins available. This is due to phase additions that are caused by time delays in op-amps and switching action. This can result in instability if sufficient phase margin is unavailable.

5.5 Hardware implementation

Figure-5.10 gives an overall depiction of the system including the fuel cell system, soft-switching boost converter, load, and duel-loop control implementation. Several considerations are necessary when it comes to practical design of a power electronics converter system. One important consideration is utilization of an appropriate gate deriver that is sufficiently fast for switching at high frequencies. Electromagnetic noise is another problem that affects the sensors and controller chip.

Negative effects of EMI can be reduced by making the traces short and placing proper filters at the inputs and outputs of the control chip.

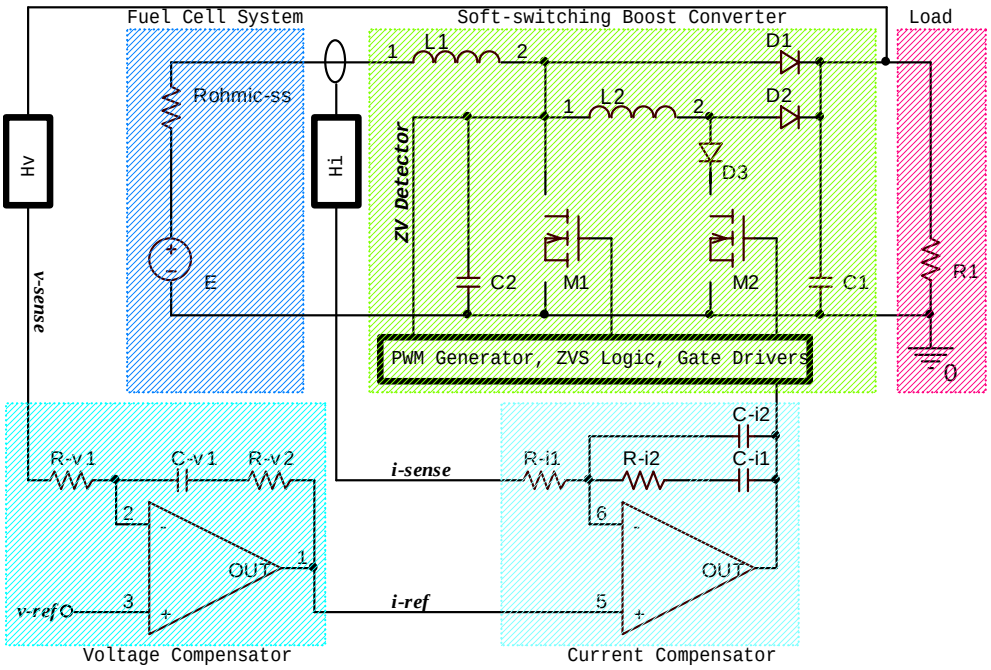

Figure-5.10 Hardware implementation of entire system

Figures-5.11 and -5.12 voltage and current waveforms were captured on the oscilloscope for the main MOSFET of hard-switching and soft-switching converters respectively. It can be seen that electrical noise is much reduced in the soft-switching converter. This is significant because the switching noise can deteriorate the signal integrity in the control chip and sensors. In this case the controller may not function as expected and this can lead to malfunction of the converter system.

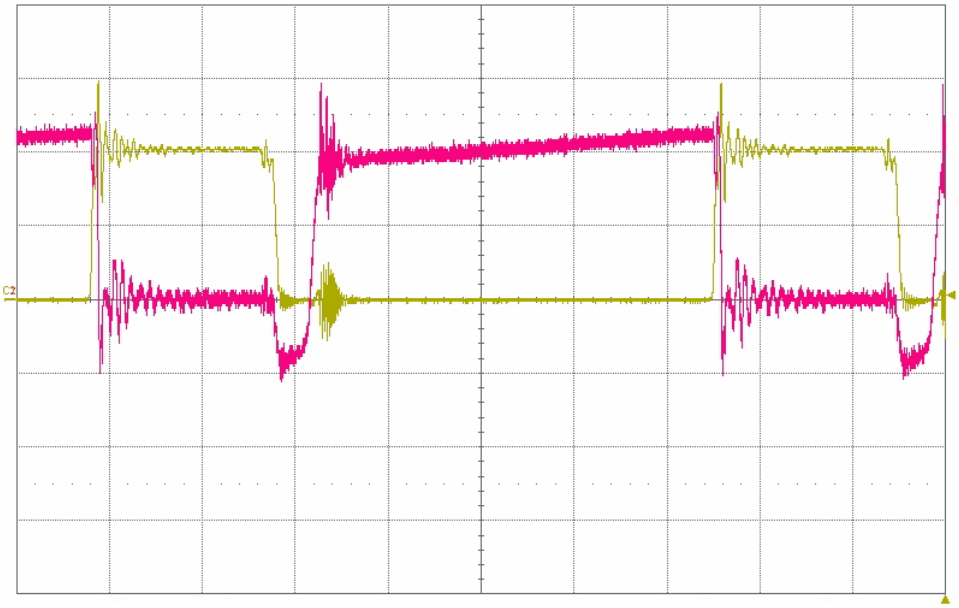

Figure-5.11 Soft-switching voltage/current waveforms of main MOSFET

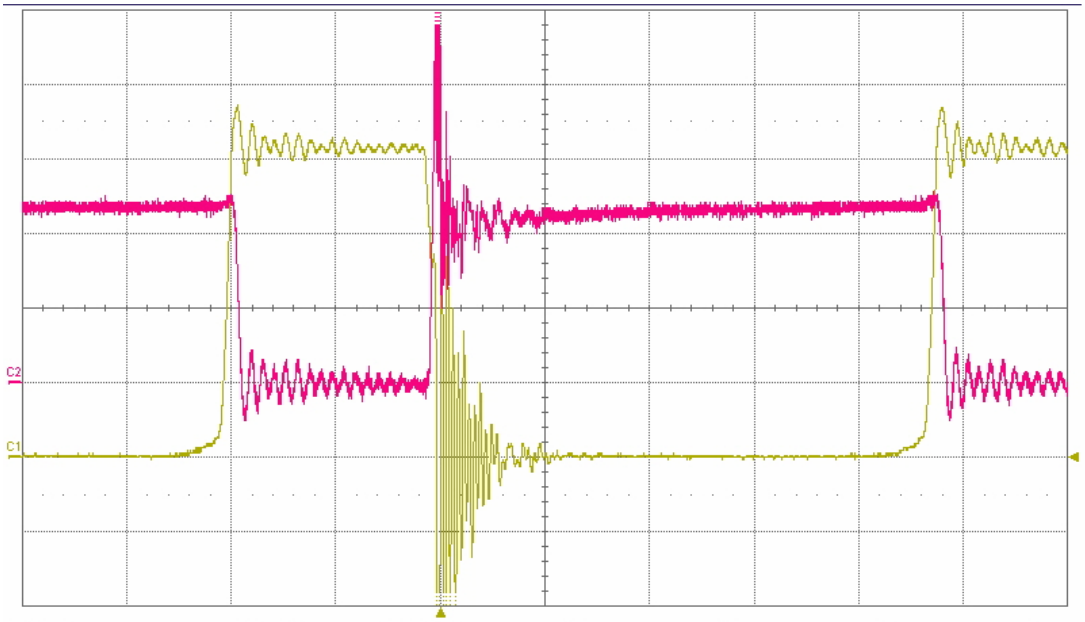

Figure-5.12 Hard-switching voltage/current waveforms of main MOSFET

CHAPTER 6

CONCLUSION

Fuel cells have numerous outstanding characteristics that make them attractive for several crucial applications. Generally, the output characteristics (steady-state and transient) of FC systems do not match the input requirements of typical loads. This is because the output voltage of these systems varies dramatically under changing load conditions. In addition FC systems are unable to operate under fast load profiles. Therefore, to effectively utilize the electrical energy generated by FC systems, power electronics converters are necessary. Also power electronics circuits should match the high-efficiency and high-power-density of FC systems.

A power electronics engineer needs an understanding of FC system's electric output characteristics in order to design an optimized power electronics module. In this thesis electrical output characteristics of a typical PEM fuel cell system was studied for the purpose of power electronics converter/inverter design. The output characteristics of a fuel cell stack which is well known does not correspond to that of the FC system because of inclusion of a control module. The main function of FC control module is to improve the overall efficiency of the system and also prevent the output voltage from fluctuating with load current. In this way, the control module improves the steady-state response of the system but deteriorates the frequency response of the system because it incorporates mechanical components.

It is shown that boost converter input characteristics match the FC systems output requirements. A high-efficient, high-power-density, low-cost, and reliable DC-DC converter topology was designed that constitutes a suitable interface between a fuel cell system and a typical application. The design goals were realized with a soft-switching boost converter by implementation of ZVS and ZCS schemes that employs a simple and effective control scheme. The results demonstrate that the use of ZVS techniques significantly improves the efficiency of high power boost converter by reducing the turn-on losses. This made possible increasing the power density of the converter by using smaller filter components, while reducing the impact switching frequency on controllers.

The converter was successfully interfaced with Nexa™ fuel cell system. Tests were performed under different load dynamics and input line disturbance. Thus, output voltage regulation and stability was verified for this converter. Additional tests were conducted to examine the load current ripple under various switching frequencies.

The following analyses were presented in this thesis: It was shown that the output current ripple of the fuel cell system decreases as the converter operates at higher frequency. This is significance because fuel cells prefer small current ripple which will result in prolonged life time of the fuel cell system. This is another benefit of operating at high frequencies in addition to achieving high efficiency, high power-density, low EMI, and low semiconductor stresses.

The following analyses were presented in this thesis:

1. State-space dynamic modeling of hard switching and soft switching boost converter
2. Efficiency calculations for hard switching and soft switching boost converter
3. State-space averaging method and small signal linearization for the purpose of frequency domain controller design

The following experiments were conducted for this thesis:

1. A complete design demonstration of a hard-switching boost converter
2. A complete design demonstration of a soft-switching boost converter
3. Efficiency measurements for both hard-switching and soft-switching converters at different operating frequencies
4. Determination of fuel cell system output characteristics such as output voltage dynamic response to load dynamics
5. A DC chopper was designed to facilitate in obtaining the fuel cell system's time constant (was found to be dependent on current frequency)
6. Successful interfacing of the converter and Nexa™ fuel cell system
7. Measurement of Nexa™ fuel cell's current ripple when connected to the Boost converters under various loads and switching frequencies

REFERENCES

1. L. B. Theodore, H. E. LeMay, B. E. Bursten, J. R. Burdge: *Electrochemistry*, 9th edition, **2003**, Pearson Education.

2. Dicks, J. Larminie: *Fuel cell system explained*, second edition, **2003**, page 67-118, Wiley.

3. H. Gregor: *Fuel cell technology handbook*, Chapter 3, **2002**, CRC Press.

4. http://www.worldcoal.org

5. S. Wang, M. Krishnamurthy, R. Jayabalan, B. Fahimi: Low-cost DC-DC converter for fuel cells with enhanced efficiency, *IEEE-Applied Power Electronics Conference (APEC)* **2006**, March 19-23, Dallas, Texas.

6. S. Wang, M. Krishnamurthy, B. Fahimi: Improved low cost Quasi-Resonant DC/DC converter for high power fuel cell systems, *IEEE-Power Electronics Specialists Conference (PESC)* **2006**, June 18-22, Jeju, Korea.

7. M. W. Ellis, M. R. Von Spakovsky and D. J. Nelson: Fuel Cell Systems: Efficient, Flexible Energy Conversion for 21st century. *Proceedings of the IEEE*, **2001**,Vol. 89, No. 12.

8. Dicks, J. Larminie: *Fuel cell system explained*, second edition, **2003**, page 1-22, Wiley.

9. Nexa™ (310-0027) Power Module User's Manual, **2003** Ballard Power Systems Inc, Page 12.

10. J. H. Hirschenhofer, D. B. Stauffer, R. R. Engleman, and M. G. Klett: *Fuel Cell Handbook 4th Ed*. Reading, PA: **1998**, Parson Inc.

11. G. Hoogers: *Fuel Cell Technology Handbook.* Boca Raton, FL, **2003**, CRC Press LLC.

12. Ballard Nexa™ Power Module User Manual, **2002**.

13. S. Caux, J. Lachaize, M. Fadel, P. Shott and L. Nicod: Modelling and control of a Fuel Cell System and Storage Elements in transport applications, *Journal of Process Control*, Vol. 15 (4), June **2005**, 481-491.

14. C. C. Wang, M. H. Nehrir, and S.R. Shaw: Dynamic Models and Model Validation for PEM Fuel Cells Using Electrical Circuits, *IEEE Transactions on Energy Conversion*, vol. 20 (2), June **2005**, 442-451.

15. Forrai, H. Funato, Y. Yanagita, and Y. Kato: Fuel-Cell Parameter Estimation and Diagnostics, *IEEE Transactions on Energy Conversion*, vol. 20 (3), September **2005**, 668-675.

16. J. Golbert and D. R. Lewin: Model-based Control of Fuel Cells, (1) Regulatory Control, *Journal of Power Sources*, vol. 135, July **2004**, 135-151.

17. J. Hamelin , K. Agbossou, A. Laperriere , F. Laurencelle, T.K. Bose, Dynamic behavior of a PEM fuel cell stack for stationary applications, *International Journal of Hydrogen Energy* , Vol. 26, October **2001**, 625-629.

18. P. Thounthong , S. Rael, B. Davat, Control strategy of fuel cell/supercapacitors hybrid power sources for electric vehicle, *Journal of Power Sources*, September **2005**.

19. M. E. Schenck, L. Jih-Sheng, K. Stanton, Fuel cell and power conditioning system interactions, Vol. 1, March **2005**, 114-120.

20. Power MOS7® Fredfet, APT50M38JFLL (Data sheet), Advanced Power Technology.®

21. Hyperfast Diods, RHRG3040 (Data sheet), Fairchild Semiconductor.®

22. Power MOS7® Fredfet, APT50M38JFLL (Data sheet), Advanced Power Technology.®

23. Hyperfast Diods, RHRG3040 (Data sheet), Fairchild Semiconductor®

24. Selection of ultra-fast recovery diodes used in flyback circuits, Dallas Semiconductor®, Nov. **2001**, 12.

25. Guerra, K. Andoh and S. Fimiani: Ulatra-fast recovery diode meet today's requirements for high frequency operation and power ratings in SMPS applications, International rectifier®

26. D. Tardiff, T. H. Barton: A summary of resonant snubber circuits for transistors and GTOs, *IEEE-Industry Applications Society Annual Meeting*, 1-5 Oct., **1989**, 1176-1180.

27. Pietkiewicz and D. Tollik: Snubber circuit and MOSFET paralleling considerations for high power boost-based power-factor correctors, *IEEE-Telecommunications Energy Conference*, 29 Oct.-1 Nov., **1995**, 41-45.

28. D. Tardiff, T. H. Barton: A summary of resonant snubber circuits for transistors and GTOs, *IEEE-Industry Applications Society Annual Meeting*, 1-5 Oct., **1989**, 1176-1180.

29. J. A. Lambert, J.B. Vieira Jr, L. C. de Freitas, M. S. Vilela, V. J. Farias: A boost PWM soft-single-switched converter without high stresses of voltage and current, *IEEE-Applied Power Electronics Conference*, 3-7 March, **1996**, 469-474

30. H. Levy, I. Zafrany, G. Ivensky and S. Ben-Yaakov: Analysis and evaluation of a lossless turn-on snubber, *IEEE-Applied Power Electronics Conference*, 23-27 Feb., **1997**, 757-763

31. W.A. Tabisz and F. C. Lee: Principle of quasi-and multi-resonant power conversion techniques, *IEEE-Circuits and Systems*, 11-14 June, **1991**, Vol 2, 1053-1056.

32. F.V.P. Robinson and B.W. Williams: Active or passive snubbing for fast switches *IEEE-Industrial Electronics Society*, 24-28 Oct., **1988**, 617-622.

33. C.-L. Chen and C.-J. Tseng, Passive lossless snubbers for DC/DC converters, *IEEE-Circuits, Devices and Systems*, 6 Dec., **1998**, 396-401

34. P. C. Todd: Subber circuits: theory, design and application, May, 1993, Unitrode® from Texas Instruments®

35. High performance power factor preregulator, UC2855A/B (data sheet), Unitrode® from Texas Instruments®

36. ZVS Average Current PFC controller, FAN4822 (application note), Fairchild Semiconductor™

37. N. Mohan, T. M. Undeland, and W. P. Robbins: *Power Electronics: Converters, Applications, and Design*. **2003**, John Wiley & Sons, Inc, Chapter 7, 3rd edition.

38. R. C. Dorf and R. H. Bishop: *Modern Control Systems*. **2005**, Pearson Education, Inc, Chapter 4, 10th edition.

39. R. D. Middlebrook and S. Cuk: A general unified approach to modeling switching-converter power stages. *Int. J. Electronics*, **1977**, Vol. 42, 521-550.

40. P. T. Krein: *Elements of Power Electronics*. **1998**, Oxford University Press, Inc, Part IV.

41. D. W. Hart: *Introduction to Power Electronics*. **1997**, Prentice Hall, Inc, Appendix B, Page 408-413.

BIOGRAPHICAL INFORMATION

Shiju Wang was born in Yanchi, China on August 23, 1972, the son of Guochen Wang and Yulan Feng. After completing the degree of B.S. from North China University of Technology, Beijing, China in 1996, he joined China Film Equipment Cooperation (Beijing) as an electrical engineer. He co-founded Beijing Huayan, Inc. in 2000 and served as the president from 2000 to 2002. During these years, he designed a series of electronic lighting ballasts for film industry. In January 2005, he entered the Graduate School of The University of Texas at Arlington.